Hyperactive mTOR signals in the proopiomelanocortin-expressing hippocampal neurons cause age-dependent epilepsy and premature death in mice

松下, 悠紀

https://doi.org/10.15017/1670405

出版情報：九州大学, 2016, 博士（医学）, 課程博士
バージョン：

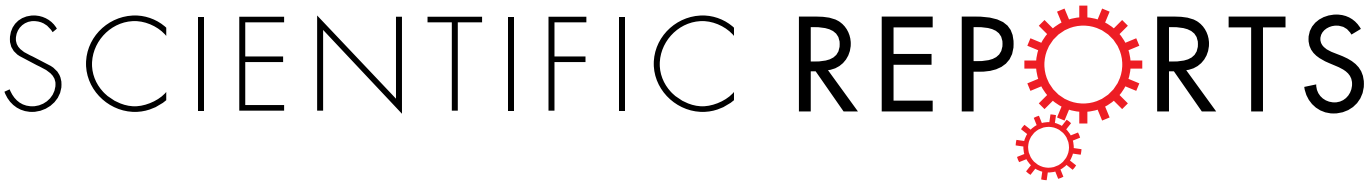

OPEN

Received: 06 January 2016
Accepted: 25 February 2016
Published: 10 March 2016

Hyperactive mTOR signals in the proopiomelanocortin-expressing hippocampal neurons cause age-dependent epilepsy and premature death in mice

Yuki Matsushita[1,*], Yasunari Sakai[1,*], Mitsunori Shimmura[2], Hiroshi Shigeto[2], Miki Nishio[3], Satoshi Akamine[1], Masafumi Sanefuji[1], Yoshito Ishizaki[1], Hiroyuki Torisu[1,†], Yusaku Nakabeppu[4], Akira Suzuki[3], Hidetoshi Takada[1] & Toshiro Hara[1,‡]

Epilepsy is a frequent comorbidity in patients with focal cortical dysplasia (FCD). Recent studies utilizing massive sequencing data identified subsets of genes that are associated with epilepsy and FCD. AKT and mTOR-related signals have been recently implicated in the pathogenic processes of epilepsy and FCD. To clarify the functional roles of the AKT-mTOR pathway in the hippocampal neurons, we generated conditional knockout mice harboring the deletion of *Pten* (*Pten*-cKO) in Proopiomelanocortin-expressing neurons. The *Pten*-cKO mice developed normally until 8 weeks of age, then presented generalized seizures at 8–10 weeks of age. Video-monitored electroencephalograms detected paroxysmal discharges emerging from the cerebral cortex and hippocampus. These mice showed progressive hypertrophy of the dentate gyrus (DG) with increased expressions of excitatory synaptic markers (Psd95, Shank3 and Homer). In contrast, the expression of inhibitory neurons (Gad67) was decreased at 6–8 weeks of age. Immunofluorescence studies revealed the abnormal sprouting of mossy fibers in the DG of the *Pten*-cKO mice prior to the onset of seizures. The treatment of these mice with an mTOR inhibitor rapamycin successfully prevented the development of seizures and reversed these molecular phenotypes. These data indicate that the mTOR pathway regulates hippocampal excitability in the postnatal brain.

Epilepsy, which affects 0.8–1% of the world's general population, is a leading cause of neurological problems in childhood[1–3]. The prevalence rate is even higher individuals with autism spectrum disorder (ASD)[4,5] and various brain malformations[6,7]. The high prevalence of epilepsy in children with these disorders has led neurologists to investigate commonalities in their genetic backgrounds. However, searching for such genetic factors is challenging because diverse sets of genetic variations are known to be associated with the onset of both epilepsy and ASD[8,9]. On the other hand, syndromic phenotypes of Mendelian disorders have provided clues to elucidate their common pathogenic mechanisms.

The mammalian target of rapamycin (mTOR) constitutes an important cascade which regulates cell growth, differentiation and metabolism. Accordingly, mTOR signaling disorders are implicated in various diseases, including cancer, epilepsy and ASD[10]. Somatic mutations in the *PIK3CA*, *AKT3* and *mTOR* genes were recently identified to cause hemimegalencephaly[11] and focal cortical dysplasia type II[12,13]. Thus these studies

[1]Department of Pediatrics, Graduate School of Medical Sciences, Kyushu University, Fukuoka 812-8582, Japan. [2]Department of Neurology, Graduate School of Medical Sciences, Kyushu University, Fukuoka 812-8582, Japan. [3]Division of Cancer Genetics, Medical Institute of Bioregulation, Kyushu University, Fukuoka 812-8582, Japan. [4]Division of Neurofunctional Genomics, Medical Institute of Bioregulation, Kyushu University, Fukuoka 812-8582, Japan. *These authors contributed equally to this work. †Present address: Department of Pediatrics, Fukuoka Dental College, Fukuoka 814-0193, Japan. ‡Present address: Fukuoka Children's Hospital, Fukuoka 813-0017, Japan. Correspondence and requests for materials should be addressed to Y.S. (email: ysakai22q13@gmail.com)

demonstrated that hyperactive mTOR signaling was involved in neuronal hypertrophy, aberrant circuit formation and epileptogenesis.

Phosphatase tensin homolog (*Pten*) encodes a lipid phosphatase that counteracts PI3K and AKT as an upstream regulator of mTOR. PTEN not only prevents overgrowth and tumorigenesis in proliferating cells, but also protects neurons from hyper-excitability and epileptogenesis[14,15]. Mouse models have been created, recapitulating progressive hypertrophy of the brain, epilepsy and autistic behaviors, which are the core symptoms of patients with Cowden syndrome and related human diseases[16,17].

Proopiomeranocortin (Pomc), the precursor peptide of adrenocorticotropic hormone (ACTH), is expressed in the particular subsets of neurons in the hippocampal dentate gyrus (DG), hypothalamic arcuate nucleus and amygdala[18]. In the hippocampal DG, for example, Pomc is only transiently expressed in newly born progenitors of granule cells and immature neurons[19,20]. It is also noteworthy that deficits in ACTH (POMC) production are implicated as an underlying cause of infantile-onset epileptic encephalopathy[21], a heterogeneous group of neuro-developmental disorders in childhood characterized by intractable epilepsy and unfavorable developmental outcomes[22]. Thus, we hypothesized that certain molecular pathways might regulate the proper expression of POMC in the hippocampus, thereby preventing the hippocampal neurons from hyper-excitability at an early stage of the postnatal brain.

In the present study, we explored the functional impact of hyperactive mTOR signaling on hippocampal neurons in the postnatal period. Using the *Cre-loxP* system, we deleted the murine *Pten* gene from hippocampal neurons expressing Pomc. All of these mice developed spontaneous seizures at postnatal week 8–10. Our data provide new lines of evidence that the deregulation of the mTOR pathway in the hippocampal Pomc-expressing neurons contributes to the onset of age-dependent epilepsy.

Results

Increased PI3K-Akt signaling in the *Pten*-cKO hippocampal dentate gyrus. We first investigated the regional expression of Pten in the *Pten*-cKO mice and their littermate controls. Immunofluorescence studies showed that Pten signals were not present in the hippocampus DG or the hypothalamus arcuate nucleus (Arc) of the *Pten*-cKO mice: whereas Pten was abundantly expressed in the control mice of the same age (Fig. 1a,b, Supplementary Fig. S1). Phosphorylated Akt (pAkt) and S6 (pS6) signals were consistently increased in these regions in the *Pten*-cKO mice, but not in the control mice (Fig. 1c). These data clearly demonstrated that the PI3K-Akt pathway hyperactivity was limited to the area of the hippocampal DG and the hypothalamus. Furthermore, quantitative Western blotting analyses showed that the pAkt and pS6 signals in the hippocampus of *Pten*-cKO mice were stronger than those in the control mice (Fig. 1d). Such differences were not observed in the cerebral cortex extracts from the *Pten*-cKO and control mice.

***Pten*-cKO mice exhibit age-dependent seizures and premature death.** The vital conditions and somatic growth of many of the brain-specific *Pten* knockout mice are reported to be severely affected from the early postnatal period[17,23]. We therefore continued to observe their gain of weight and general activity. Our *Pten*-cKO mice grew normally and their body weight gain was not significantly different to that of control mice (Supplementary Fig. S1). Although the appearance of the brain in *Pten*-cKO mice did not differ from that of control mice, the whole brain was significantly heavier ($n = 18$ and 15, respectively. $P = <0.0001$, Wilcoxon rank sum test, Supplementary Fig. S1). We serially examined the brain sections of the control and *Pten*-cKO mice at 4, 6 and 8 weeks of age. We noticed that the hippocampus of the *Pten*-cKO mice gradually became enlarged and distorted in an age-dependent manner (Fig. 1e, Supplementary Fig. S1).

Notably, all ($n = 31$) of the *Pten*-cKO mice became hypersensitive and began to show a rigid posture with startle responses to the routine handling during cage exchange from 8 weeks of age. Ninety-seven percent (30 of 31) of these mice died by the tenth week of age (Fig. 1f). Since epilepsy is commonly observed in ASD patients and animal models[4,24], we wondered whether the sudden onset of this phenotype might be associated with abnormal neuron excitability. Indeed, in *Pten*-cKO mice, the hippocampal DG expressed significantly higher levels of cFos, a neuronal activity marker, than in control mice of the same age ($P = 0.0028$, Fig. 1g,h). Neuropeptide Y (Npy) was over-expressed at this age in the DG of the *Pten*-cKO mice in comparison to the control mice ($P < 0.0001$, Fig. 1g,h). We also verified that there were no sex differences in the age of onset or morbidity between the control and *Pten*-cKO mice. Double-heterozygous mice (*Pomc-Cre*$^{Tg/+}$;*Pten*$^{flox/+}$) did not show the seizure phenotype, which excluded the deleterious effects of *Pomc-Cre* transgene ($n = 13$). These data strongly suggested that the congenital loss of *Pten* in the DG might cause a highly penetrant phenotype of epilepsy in mice at the eighth to tenth week of age.

***Pten*-cKO mice present spontaneous seizures at eight to ten weeks of age.** When closely inspecting the behaviors of *Pten*-cKO mice under video monitoring, we found that recurrent seizures began to occur at 8–10 weeks of age. These seizures were classified into two types: an immobile state with unresponsiveness (Fig. 2a left, Supplementary Video S1) and generalized tonic-clonic convulsions accompanying intermittent falls and jumping (Fig. 2a right, Supplementary Video S2). We thus conducted simultaneous video-electroencephalography (EEG) recordings of *Pten*-cKO mice at 8–10 weeks of age after the insertion of stereotactic electrode. Two channels of electrodes were used to monitor the electrical activity of the hippocampus and cerebral cortex (Supplementary Fig. S2). Epileptiform discharges rarely appeared in the interictal phase (Fig. 2b), whereas ictal patterns of rhythmic sharp waves, poly-spikes (Fig. 2b, blue square), and periodic suppression and burst patterns of epileptiform discharges (Fig. 2c, blue square) emerged concurrently with the seizures (Racine's score at IV/V).

No preceding epileptiform discharges were evoked in the hippocampus prior to the activation of the cerebral cortex. Thus it was suggested that epileptogenic circuits between the two regions already existed when the

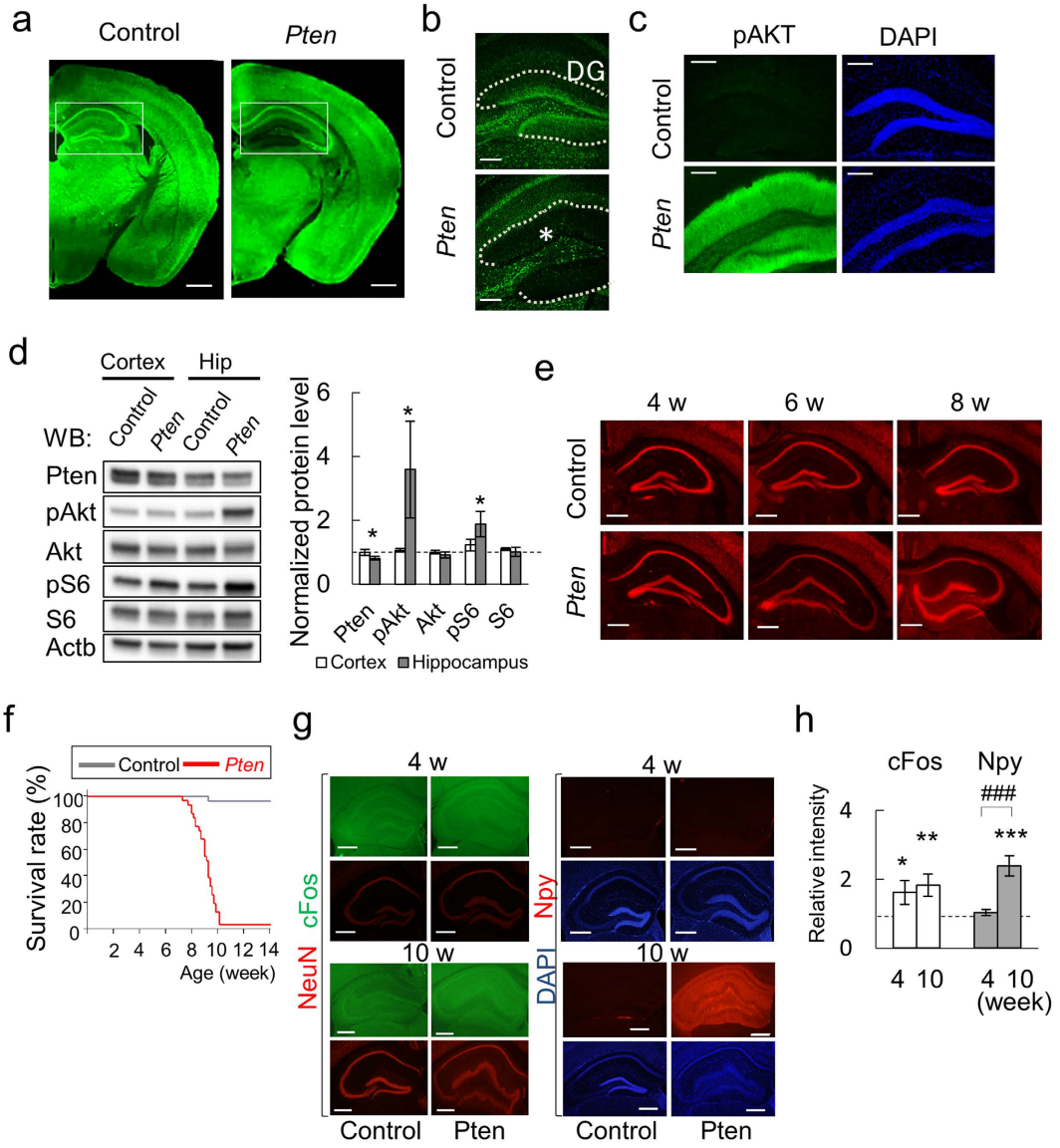

Figure 1. The characteristics and morphological findings of *Pten*-cKO mice. (**a**) Immunofluorescence studies on Pten expression (green). The left two panels show the coronary brain sections from control (left) and *Pten*-cKO (right, *Pten*) mice at 4 weeks of age. The squares denote the areas of the hippocampus DG. Scale bar, 1 mm. (**b**) Confocal images with a higher magnification of the DG. Asterisk indicates the loss of Pten signals (green) in the granule cell layer of DG (dashed lines). Scale bar, 200 μm. (**c**) Hyperactive AKT signaling in the DG of *Pten*-cKO mice. The immunofluorescence signals of the phosphorylated S473 of AKT (pAKT, green) and DAPI (blue) are shown. Scale bar, 200 μm. (**d**) Western blotting of the cerebral cortex and hippocampal extracts from control and *Pten*-cKO mice at 8 weeks of age. The bar plots for the relative expression levels of the indicated proteins are shown in the right panel. Note that increased pAKT and pS6 signals are seen in the hippocampus, but not in the cerebral cortex of *Pten*-cKO. *$P < 0.05$ ($n = 4–6$, Wilcoxon rank sum test). (**e**) Progressive hypertrophy of the DG in *Pten*-cKO mice. The morphological changes of the DG hippocampal sections at the ages of 4, 6 and 8 weeks. See Supplementary Fig. S1 for the whole brain images. Scale bar, 500 μm. (**f**) Survival rates (%) of control and *Pten*-cKO mice. (**g**) cFos (green) and NeuN (red) expression (left panels). Npy (red) and DAPI (blue) expression (right panels), in the DG at 4 and 10 weeks of age. Scale bars, 500 μm. (**h**) The quantitated results of (**f**,**g**). The relative signal intensity (*Pten*-cKO/control) of cFos and Npy at 4 and 10 weeks are plotted. Asterisks indicate significantly higher levels of cFos and Npy expressions in the DG of Pten-cKO mice in comparison to the control mice. $P < 0.05$, **$P < 0.01$, $^{###}$ and ***$P < 0.001$ ($n = 4–16$, Wilcoxon rank sum test).

Pten-cKO mice exhibited seizures. To biochemically establish whether the hippocampus was the epileptogenic origin in our *Pten*-cKO mice, we examined whether hippocampal *cFos* expression might precede the phenotypic onset of seizures. The time course of *cFos* expression showed that *cFos* mRNA was robustly induced in the hippocampus of the *Pten*-cKO mice at 8 weeks of age: it was not induced in the cerebral cortex (Supplementary Fig. S3). Increased *cFos* expression in the cerebral cortex was observed at 9–10 weeks of age, during the period of the

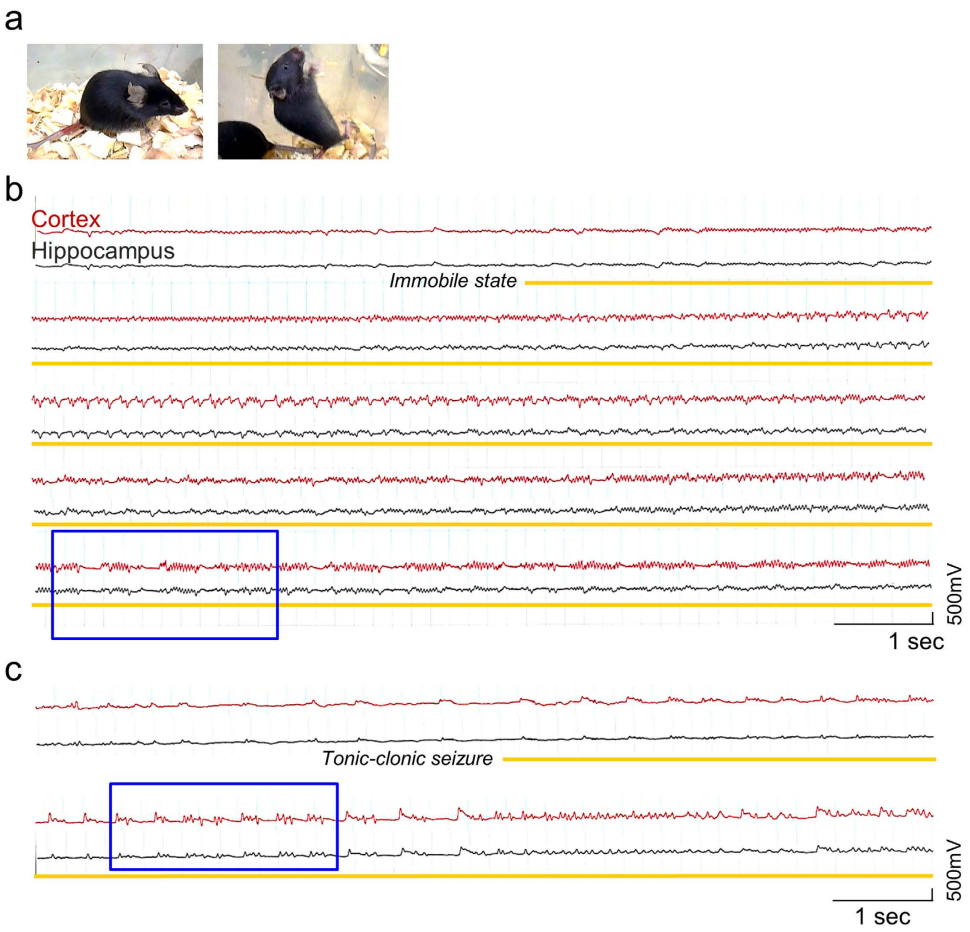

Figure 2. Video-monitored EEG recordings of seizures in *Pten*-cKO mice. (**a**) *Pten*-cKO mice in static (left) and generalized tonic-clonic seizures (right). (**b,c**) Representative EEG traces associated with seizures in *Pten*-cKO mice. Cortical (red) and hippocampal (black) electrodes detected the transition of resting background activity evolving into the paroxysmal phase (yellow lines). Blue squares denote intervals, in which high-amplitude, rhythmic poly-spike (**b**) or periodic bursts (**c**) are seen.

phenotypic onset of seizures (Supplementary Fig. S3). Such transcriptional activation was never observed in the hippocampus or the cerebral cortex of the control mice.

The excitatory-inhibitory synaptic imbalance in the hippocampus of *Pten*-cKO mice. To gain insight into the molecular bases for the age-dependent seizures that occurred in our *Pten*-cKO mice, we tested whether excitatory-inhibitory (EI) imbalances might contribute to their pathogenic process. Serial immunofluorescence studies revealed that the DG of *Pten*-cKO expressed significantly higher levels of excitatory synapse markers, Homer and Psd95, in parallel with an astroglial marker, Glial fibrillary acidic protein (Gfap), than the control mice by 6 weeks of age ($P = 0.021$, 0.0004, 0.0011, respectively; Fig. 3a,b). On the other hand, Gad67, a GABAergic interneuron-specific marker was expressed at a lower level in the hilus region of the DG of the *Pten*-cKO than in control mice ($P = 0.2817$, Fig. 3a,b). The time course of these data supported that the differential expressions of excitatory and inhibitory neurons in the DG of the *Pten*-cKO mice were already evident prior to the onset of seizures (Fig. 3b), suggesting that the excitatory and inhibitory imbalance might be a prerequisite for the epileptogenic condition of the *Pten*-cKO mice. Western blotting also supported the expression levels of Homer and Shank3 were significantly higher in the hippocampus of the *Pten*-cKO mice than in the control mice at 8 weeks of age, but not at 2 weeks of age (Fig. 3c,d).

Age-dependent hypertrophy of the dentate gyrus neurons in *Pten*-cKO mice. We investigated whether the progressive EI imbalance in the DG of *Pten*-cKO mice might be chronologically associated with its morphology after birth. To distinguish hypertrophy of the differentiated neurons from overly proliferating stem cells, we performed bromodeoxyuridine (BrdU) labeling of the neural stem cells in the DG, and compared the numbers in the *Pten*-cKO and control mice at 2 and 4 weeks of age. Contrary to our prediction, there was no difference in the number of proliferating neural stem cells in the *Pten*-cKO and control mice (Fig. 4a). The microtubule-associated protein 2 (Map2)-labeled dendritic shafts of neurons in the molecular layer in the *Pten*-cKO mice were observed to be significantly thicker than in control mice (Fig. 4b, upper and Supplementary Fig. S4). NeuN-positive neurons in the granular cell layer (GCL) showed a significantly larger soma (Fig. 4b,

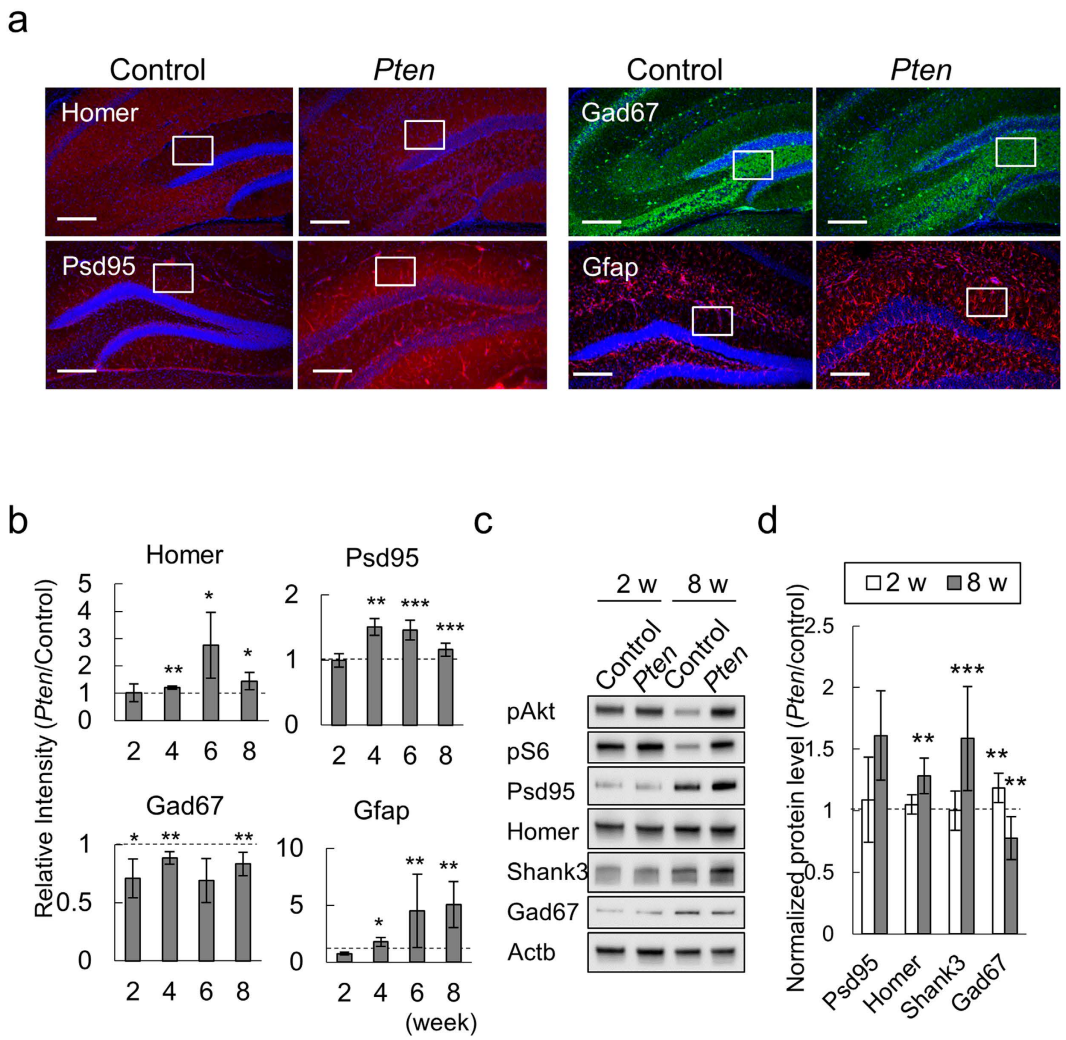

Figure 3. Excitatory-inhibitory imbalance in the hippocampus of *Pten*-cKO mice. (**a**) The expression of excitatory synapse (Homer, Psd95), inhibitory neuron (Gad67) and glial markers (Gfap) in the hippocampus of control and *Pten*-cKO mice at 6 weeks of age. Immuno-labeled proteins are annotated. Squares indicate the ROIs for the quantitative analyses. Scale bar, 200μm. (**b**) The quantitated results of the immunofluorescence studies. The relative fluorescence intensity (*Pten*-cKO/Control) of Homer, Psd95, Gad67 and Gfap are plotted for 3 or more independent pairs of *Pten*-cKO and control littermates at each time point. Horizontal dashed lines indicate the reference values of the control mice. (**c**) Representative images of western blots for the hippocampal extracts. Three or more pairs of control and *Pten*-cKO mice at 2 and 8 weeks of age were used for this study. (**d**) The quantitated Western blotting data. Bar plots for the relative expression (*Pten*-cKO/Control) of the indicated proteins. The plotted values show the means ± SD ($n \geq 3$). In panels (**b,d**), *$P < 0.05$, **$P < 0.01$, ***$P < 0.001$.

lower). We thus considered that the hypertrophy of the *Pten*-cKO DG was mainly the result of aberrant neuronal differentiation, and had not been caused by an excess of self-proliferating neural stem cells.

To dissect the differentiation process of progenitor cells, we consecutively analyzed the cell populations by immuno-labeling for doublecortin (Dcx) and Gfap in *Pten*-cKO and control mice at 2, 4, 6 and 8 weeks. At two weeks of age, the numbers of Gfap and Dcx-positive cells in the *Pten*-cKO mice did not differ from the control mice (Fig. 4c). As previously mentioned, the numbers of Gfap-positive cells in the DG of the *Pten*-cKO mice were increased at 6–8 weeks of age (Figs 3b,4d and Supplementary Fig. S5). On the other hand, the number of Dcx-positive progenitor cells in the *Pten*-cKO mice decreased to 65% of the number in the control mice at 6 weeks of age (Fig. 4c–e and Supplementary Fig. S5). Another prominent feature was the Dcx-positive progenitors were dispersed in the DG of *Pten*-cKO mice at 6–8 weeks of age. These data indicated that loss of *Pten* in the hippocampal DG disturbed neuronal differentiation.

The improper differentiation of neuronal progenitor cells prompted us to investigate whether *Pten*-cKO mice might develop abnormal neural circuits after birth. To confirm this, we analyzed the sprouting patterns of mossy fiber, the outward axon from the granule cells of the DG, projecting to the CA3 region[25]. An immunofluorescence study with an axonal marker, Znt3, verified that the mossy fibers in the hilus region in both control and *Pten*-cKO

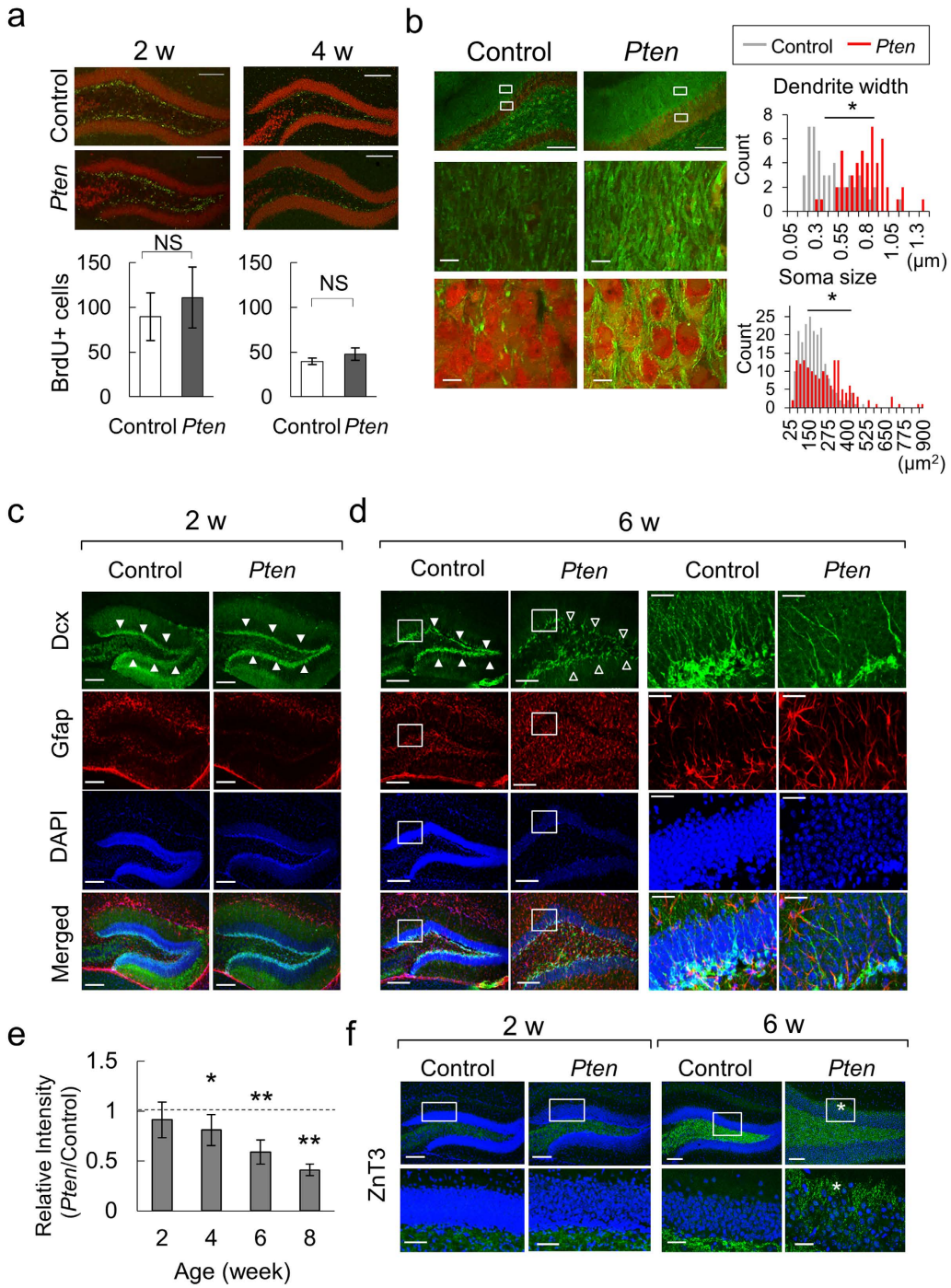

Figure 4. Hypertrophy of the DG and dysmorphic neurons in *Pten*-cKO mice. (**a**) BrdU (green) and NeuN (red) signals in the DG of the control and *Pten*-cKO mice at 2 and 4 weeks of age. The number of BrdU-positive cells in the subgranular zone are plotted (means ± SD values, n = 3). NS, not significant. Scale bars (**a–d**) denote 200 μm unless otherwise stated. (**b**) Hypertrophy of the DG neurons in the *Pten*-cKO mice. Left images show Map2 (green) and NeuN (red) signals. Histograms represent the counts for indicated widths of dendritic shafts (right upper, 50 for control and 50 for *Pten*-cKO) and the sizes of soma (right lower, 200 control and 160 *Pten*-cKO) from 3 pairs of littermates are shown. *$P < 0.0001$. Scale bars (lower panels), 10 μm. (**c,d**) Aberrant differentiation of neuronal progenitors in the DG of *Pten*-cKO. Dcx (green), Gfap (red) and DAPI (blue) signals are shown. Filled arrowheads indicate the Dcx signals peaked at the subgranular zone. Lucent arrowheads point to the sparse patterns of the Dcx signals at 6 weeks of age (d, *Pten*-cKO). Higher magnification views are provided for the boxed (d, far-right two columns). Scale bars, 20 μm (**d**) higher magnification images). (**e**) The relative fluorescence intensity (*Pten*-cKO/control) of Dcx in the subgranular zone at 2, 4, 6 and 8 weeks of age (mean ± SD, n ≥ 3). (**f**) Znt3 (green) and DAPI (blue) signals in DG at 2 and 6 weeks of age. Asterisks indicate the presence of abnormal sprouting of mossy fibers. The lower panels show higher magnification views of the boxed areas. Scale bars, 50 μm (lower panels).

mice were normal at 2 weeks of age (Fig. 4f, left). However, the Znt3 signals of the *Pten*-cKO mice penetrated the granule cell layer and the fibers extended to reach the molecular layer at 6 weeks of age (Fig. 4f, right). Thus, our microscopic data confirmed that the regional *Pten* deletion in the Pomc-expressing neurons caused impaired neuronal differentiation in the DG, which was accompanied by progressive hypertrophy and excessive excitatory synapse components after birth. Moreover, the aberrant morphology of differentiating neurons in the DG coincided with abnormal patterns of dendritic polarity and mossy fiber sprouting from granule cells. These data indicated that the hippocampus of the *Pten*-cKO mice already formed epileptogenic circuits prior to the onset of seizures.

Neuroendocrine dysfunctions in the hippocampus of *Pten*-cKO mice. We further sought the mechanisms that disturbed the homeostasis of the EI balance in our *Pten*-cKO mice. Adrenocorticotropic hormone (ACTH), a cleavage product of POMC, is the most effective therapeutic agent for treating epileptic encephalopathy in childhood[22]. We therefore hypothesized that our *Pten*-cKO mouse might be a relevant model of the deregulation of the corticotropin releasing hormone (CRH) - ACTH axis.

We analyzed the expression of *Crh* and *Pomc* mRNAs in the hippocampus of *Pten*-cKO mice at different time points before and after the onset of seizures, and compared them with control mice. We found that the hippocampus of the *Pten*-cKO mice already expressed significantly higher levels of *Crh* mRNA at 8 weeks of age (8 vs. 4 weeks of *Pten*-cKO, $P = 0.0034$, Supplementary Fig. S6). The *Crh* expression rose even higher after the onset of seizures (9–10 vs. 4 weeks, $P = 0.0058$, Supplementary Fig. S6). In contrast, *Pomc* expression declined in the hippocampus of the *Pten*-cKO mice as they grew older, but remained unchanged in the hippocampus of control mice. Consequently, the *Pten*-cKO mice expressed significantly lower levels of *Pomc* mRNA after the onset of seizures than they did before the onset of seizures (9–10 vs. 4 weeks, $P = 0.0137$, Supplementary Fig. S6). There was also a significant difference in the Pomc expression of the *Pten*-cKO and control mice at 9–10 weeks of age. The loss of *Pten* in the hippocampus did not affect *Crh* expression in the cerebral cortex or the hypothalamus (Supplementary Fig. S6), which excluded the possibility that increased *Crh* in the hippocampus was only a secondary effect. These findings indicated that the loss of *Pten* in the Pomc-positive neurons disturbed the regulation of *Crh* and *Pomc* expression in the developing hippocampus, rather than in the hypothalamus or cerebral cortex. It was also consistent with a feedback-loop model of elevated CRH due to the decreased synthesis of ACTH (POMC/MSH) in the pathogenic condition of human epileptic encephalopathy[21].

Nonetheless, genetic expression and subsequent releases of neuropeptides from cells are known to fluctuate with circadian rhythm and other chronological factors[26]. It was therefore a possibility that the subtle differences in the expressions of neuropeptides be a consequence of variable conditions in the analysis. We therefore analyzed the co-expression profiles of *Crh* with *Crh receptor 1* (*Crhr1*) at 8–10 weeks. Intriguingly, the *Crh-Crhr1* correlation plots showed distinct patterns of co-expression in the 3 regions that were tested in the control and *Pte*n-cKO mice (Supplementary Fig. S6). These data convinced us that both an excess of Crh and a shortage of Pomc became prominent in the hippocampus of the *Pten*-cKO mice at the age of onset (8–10 weeks), but not before (4–6 weeks of age).

To assess the functional relationship between mTOR hyperactivity and the deregulated Crh-ACTH axis in our *Pten*-cKO mice, we attempted to control the seizures by treating them with serial intraperitoneal injections of ACTH (ACTH 1–24, Sigma A0298, 0.0125 mg/kg/day for seven consecutive days at 8 weeks of age). However, the ACTH therapy did not improve their seizures or mortality rate (our unpublished results). It was therefore unlikely that neuroendocrine deficits played a major role in the onset of epileptic seizures in our *Pten*-cKO mice.

Rapamycin restores the epileptogenic phenotypes of *Pten*-cKO mice. Lastly, we determined whether the epilepsy of the *Pten*-cKO mice could be mitigated by controlling the hyperactive mTOR signaling with its inhibitor rapamycin. *Pten*-cKO mice were treated with vehicle or rapamycin from 6 to 9 weeks of age, and their brains were subjected to Western blotting and immunofluorescence studies. We found that the rapamycin-treated brains weighed significantly less than vehicle-treated brains ($P = 0.0015$, Supplementary Fig. S7). Rapamycin successfully prevented *Pten*-cKO mice from developing seizures, and the seizure-free survivals of the vehicle and rapamycin-treated *Pten*-cKO mice were 0% (0 of 11) and 82% (9 of 11), respectively ($P < 0.0001$, Fig. 5a). Western blotting showed that rapamycin treatment suppressed the increased pAKT and pS6 signals in the hippocampal extracts from the *Pten*-cKO mice to the level of the control mice (Fig. 5b, Supplementary Fig. S7). More intriguingly, the expression of Homer and Shank3 was normalized to the control level.

Microscopic data also supported that the treatment with rapamycin suppressed the hypertrophy of the DG as well as the excessive pAKT signaling in *Pten*-cKO mice (Fig. 5c: NeuN and pAKT). We verified that the loss of Pten expression in this region did not differ in the treatment and non-treatment groups (Fig. 5c: Pten). Rapamycin treatment led to a recovery of Dcx expression with peak signal intensity at the subgranular zone of the DG (Fig. 5c: Dcx). Concordant with these data, rapamycin blocked the abnormal protrusion of mossy fibers into the granule cell layers (Fig. 5c: Znt3). Regarding the EI imbalance in the *Pten*-cKO mice, the abnormal distribution of Gfap, Homer and Psd95 in this area was corrected (Fig. 5d: Gfap, Homer and Psd95). While the expression of interneuron marker, Gad67, was significantly reduced, the reactive expression of Npy was nearly completely absent from the DG after rapamycin treatment (Fig. 5d: Gad67 and Npy). Lastly, we verified that rapamycin suppressed the expression of cFos, indicating that the treatment successfully controlled the excitability of the DG neurons in the *Pten*-cKO mice.

Discussion

Our *Pten*-cKO mice developed spontaneous seizures at a relatively mature stage (8–10 weeks) in comparison to brain-wide or DG neuron-specific knockout mice[16,17,24,27]. Among the various types of brain-specific *Pten* knockout mice, our *Pten*-cKO mice resembled those of previous reports[28,29]. Our experimental data recapitulated their

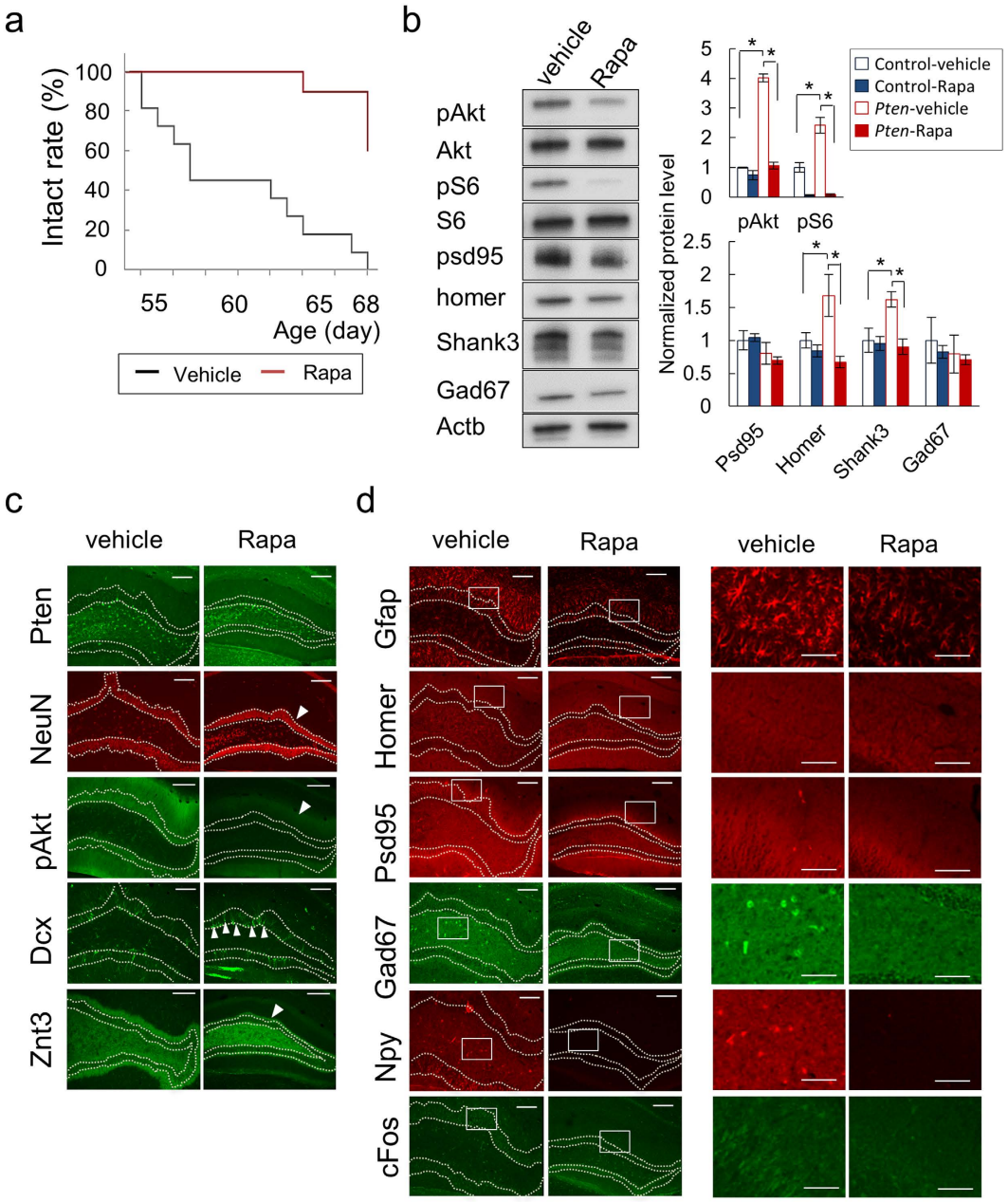

Figure 5. The postnatal treatment of *Pten*-cKO mice with rapamycin extends their intact survival and normalizes their molecular phenotype. (**a**) Intact survivals (%) of *Pten*-cKO mice with vehicle or rapamycin (Rapa) treatment. (**b**) Western blotting for the hippocampal extract from vehicle- or rapamycin-treated *Pten*-cKO mice. The bar plots show the quantitative results (mean ± SD) of Western blotting from 3 pairs of mice with or without rapamycin treatment. The expression level of the control mice after the vehicle treatment was set as 1 (reference). *$P < 0.05$. (**c,d**) Immunofluorescence images of the DG from vehicle or rapamycin-treated *Pten*-cKO mice at 9 weeks of age. The arrowheads indicate the presence of neurons in which the expression of annotated proteins recovered after rapamycin treatment (**c**). Higher magnification images of the boxed areas are provided in the two columns on the right (**d**). Dashed lines denote the boundaries of the granule cell layers of the DG (**c,d**). Scale bar, 200 μm and 100 μm ((**d**) higher magnification).

major findings and showed some novel findings: 1) the inborn deletion of *Pten* in the hippocampal DG was sufficient to cause severe epilepsy in adulthood; 2) the hyperactive mTOR signaling pathway disrupted Crh-ACTH homeostasis in the hippocampus; and 3) postnatal treatment with rapamycin not only reversed the seizure phenotype, but also corrected the molecular phenotypes of the excessive production of ASD-associated proteins, such as Shank3 and Homer.

Ljungberg *et al.* demonstrated the value of neuron subset-specific *Pten* knockout mice as an animal model for focal cortical dysplasia (FCD) and the antiepileptic effects of rapamycin[28,29]. Since our *Pten*-cKO mice harbored genetic mosaicism, which resulted in the chimeric expression of *Pten* in their brain, they can be also regarded

as a disease model for congenital disorders with hyperactive AKT-mTOR conditions due to somatic mutations. Patients with FCD, a brain malformation, suffer from intractable epilepsy in childhood and early adulthood[30]. The diagnostic categories of FCD are based on distinct features in neuroimaging studies and the histopathological findings of surgically resected tissues[31]. Among these categories, FCD type II is characterized by the presence of cytomegalic dysmorphic neurons and balloon cells[30,32].

Both cytomegalic dysmorphic neurons and balloon cells have been considered analogous to giant cells in the tuberous sclerosis complex (TSC), which is another example of a Mendelian disorder which causes epilepsy and developmental problems in childhood. Indeed, recent studies have shown balloon cells to be characteristically hyperactive in the mTOR pathway[33]. In line with these biological notions, recent evidence has shown that balloon cells carry somatic mutations in genes encoding components of the AKT-mTOR pathway[12,13]. Moreover, these cells have been suspected to function as generators of paroxysmal activity in epileptogenic origin[34]. Thus, it was reasonable that our *Pten*-cKO mice exhibited age-dependent seizures associated with regionally hyperactive AKT-mTOR signals in the hippocampus, wherein the *Pten*-deficient hypertrophic neurons were likely epileptogenic sources.

It remains controversial, however, whether our *Pten*-cKO mice can be considered as a new model for FCD. Alternatively, they may be a better fit for a phenotype of temporal lobe epilepsy (TLE) in adulthood[35]. Although the majority of cases with TLE are known to show hippocampal atrophy or sclerosis, earlier studies using biopsy and autopsy samples demonstrated the hypertrophy of hippocampal DG neurons[36]. More notably, hypertrophy of the DG in TLE patients appeared to show sparsely scattered appearance of DCX-positive immature neurons[37] and accelerated AKT-mTOR signaling[38]. Thus, excessive AKT-mTOR signaling might contribute to the neuronal hypertrophy of the DG neurons at an early stage of TLE, while they eventually follow the course of degeneration with additive effects of chronic excitotoxicity, secondary inflammations and other molecular mechanisms. To validate this hypothesis, it could be worth testing whether the hypertrophic neurons in our *Pten*-cKO mice will eventually exhibit sclerotic degeneration when they are successfully rescued to survive after the onset of seizures.

Aberration of the Crh-ACTH axis has been implicated in the onset of infantile spasms (IS), the most prevalent form of epileptic encephalopathy in infancy[21]. We thus initially hypothesized that loss of *Pten* in Pomc-expressing neurons could reproduce child-onset seizures that resemble the phenotypes of humans. However, our *Pten*-cKO mice did not show such early-onset seizures. These data raised two possibilities: that the Pomc-positive neurons of the hippocampus might be irrelevant to the pathogenic process of IS: or that the hippocampal neurons could be relevant, but insufficient to drive similar phenotypes in mice. We emphasize the value of the latter hypothesis because previous studies supported this concept. For example, a clinical study using single photon emission tomography revealed decreased regional cerebral blood flow in the hippocampus of IS patients[39]. In rodents, ACTH was shown to regulate the hippocampal expressions of *Crh* and *Crhbp*[40]. Furthermore, considering the various types of mouse models of IS that have been generated to date, their ages of onset and seizure patterns did not necessarily correlate to those of humans. These findings pointed to the fact that the creation of rodent models of IS remains challenging due to technical difficulties[41].

The cleavage product of POMC, alpha-melanocoritin stimulating hormone (alpha-MSH), exerts anorectic functions through its binding to central melanocortin receptors (MCRs) that are expressed in the hypothalamic arcuate nucleus[42]. Different types of MCRs are also expressed in the central nervous systems of mammals. Among them, MC3R and MC4R have been reported to bind to both ACTH and MSH, and to modulate hippocampal synaptic plasticity[43]. Intriguingly, the functional loss of MC4R resulted in cognitive dysfunctions, suggesting the indispensable roles of MSHs and ACTH for cognitive development in childhood[44]. Moreover, early intervention with ACTH treatment has been shown to have benefits on the long-term prognosis of seizures as well as cognitive development in children affected by IS[45].

In this study, we found that the loss of *Pten* not only caused a regional EI imbalance and impaired the differentiation of neuronal progenitors, but that it also disturbed the synthesis of *Pomc* itself in the hippocampus after birth. These data collectively suggested that the mTOR pathway in Pomc-expressing neurons might contribute to both cognitive development and epileptogenesis.

We found that the postnatal treatment of our *Pten*-cKO mice with rapamycin was effective for preventing the onset of their epilepsy. Recent studies have also shown that administration of mTOR inhibitors ameliorated epilepsy in FCD and tuberous sclerosis[46,47]. These data indicate that the homeostatic regulation of the mTOR signals is essential for the development of functional connectivity in the postnatal brain. However, it is unclear how the hyperactive mTOR pathway contributes to the formation of epileptogenic circuits in a certain period of childhood. Both cell-intrinsic and non-intrinsic models have been proposed as epileptogenic mechanisms in FCD[48,49]. In this study, we found that the expression levels of ASD-associated proteins, such as Shank3 and Homer, fluctuated according to the hyperactive or normally-regulated conditions of the mTOR signals. Thus, it can be hypothesized that hyperactive mTOR signals might lead neurons to become hyper-connective through the excessive biogenesis of excitatory synapses, as proposed in the pathogenic model for the ASD brain[50,51]. These findings appeared to be consistent with those of our previous studies, which predicted that the Shank-Homer protein complexes might regulate the activity of the mTOR pathway in the postsynaptic compartments[52]. *Pten* and *Shank* double mutants will clarify the functional roles of ASD-associated proteins in the development of epilepsy in adults.

Children with tuberous sclerosis complex are highly susceptible to IS, while they develop ASD later in childhood[53]. Thus, one could speculate that the pathogenic processes underlying epileptic encephalopathy may share common molecular pathways with ASD, but that such molecular pathways may contribute to the phenotypic onsets through distinct subsets of neurons or differential brain regions. Identifying downstream molecular pathways, such as the AKT-FOXG1 axis, will be the key to elucidating the reason why developmental delay and autism are common sequelae in patients with IS and other forms of epileptic encephalopathy[46].

In conclusion, this study disclosed that the Pomc neuron-specific loss of *Pten* was sufficient to cause age-dependent seizures in mice. This study also supported that hyperactive mTOR signaling contributed to the

development of epileptogenic circuits through the overproduction of excitatory synapse-associated proteins. Searching for events downstream of the mTOR pathways will provide further benefits in future translational research for patients with FCD and associated diseases.

Materials and Methods

Ethics statement. All experimental methods were carried out in accordance with the approved guidelines by Institutional Review Board and licensing Committee at Kyushu University (#23–53). All of the mouse experiments were performed according to guidelines and protocols which were approved by the Kyushu University Institutional Animal Care and Use Committee (#A-25–006).

Animals. Mice were housed in a specific pathogen-free environment and maintained in a C57BL/6 J background. The animals had *ad libitum* access to food and water at all times, the temperature was maintained at 25 °C with a 12-h light-dark cycle. Sex-matched littermates were used for the pairwise comparison of immunofluorescence and Western blot analyses. The following mouse lines were used: *Pten-loxP* mice[54] and *proopiomelanocortin* (*Pomc*) promoter-driven *Cre* transgenic mice (*Pomc-Cre*$^{Tg/+}$)[55]. *Pomc-Cre* transgenic (Tg) mice were purchased from Jackson Laboratory (Bar Harbor, ME, USA). Details for mating scheme are summarized in Supplementary Fig. S1. Littermates without the *Pomc-Cre* allele (*Pomc-Cre*$^{+/+}$;*Pten*$^{flox/flox}$) were used as controls. The primers that were used for genotyping are provided in Supplementary Methods.

Video-monitoring EEG. Deeply anesthetized 8-week-old *Pten*-cKO mice underwent the chronic implantation of EEG electrodes, as previously described[56]. Electroencephalograms (EEG), which were recorded by the surface and depth electrodes, were analyzed (PowerLab/8sp, AD Instruments, Bella Vista) and stored using a commercial personal computer-based system, NB75H (Fujitsu, Tokyo). The animals' behavior was monitored with a digital video camera (DCR-TRV9NTSC, Sony, Tokyo) for 8 hours per day. Epileptiform discharges were determined as clear high amplitude spikes and rhythmic waves or polyspikes[56]. Details in surgical procedures for electrode placement are described in Supplementary Methods.

Quantitative real time PCR. Isolated brains were immediately cut on ice to separate the cortex, hippocampus, and hypothalamus. The dissected tissues were snap-frozen in liquid nitrogen and stored until use at −80 °C. Total RNA was extracted with an RNeasy Mimi Kit (Qiagen) for isolated frozen tissues. Complementary DNA was synthesized using a High-Capacity RNA to cDNA Kit (Life Technologies) according to the manufacturer's protocol. A quantitative real time PCR (qRT-PCR) was performed using Fast SYBR Green Master Mix (Life Technologies) with custom primers (Supplementary Table S1) and a TaqMan Gene Expression Assay (Life Technologies) to identify *Pomc* expression, using the StepOnePlus system (Life Technologies). Mouse *Actb* was used as an internal control. Relative gene expression was calculated by the ddCt method.

Immunofluorescence study. Immunofluorescence studies were performed as previously described[57]. Briefly, animals were deeply anesthetized and perfused with 4% paraformaldehyde (PFA) in phosphate buffered saline (PBS). The brain was removed and immersed in 4% PFA overnight. The fixed brains were cryo-protected with 20 and 30% sucrose-containing PBS at 4 °C for 24 hours each, and frozen in O.C.T. compound (Sakura Finetek, Tokyo). Fixed samples were serially cut at 40 μm of thickness. Sections were blocked with Block Ace (Morinaga, Japan) and incubated overnight at 4 °C with primary antibodies (See Supplementary Table S2 for the list of primary antibodies). Alexa-488 and 555 (Life Technologies, Carlsbad, CA) were used for the secondary antibodies. DAPI was used for nuclear staining. The signal intensity of an immuno-labeled protein in the region of interest (ROI) was measured for a quantitative analysis using the NIS-elements AR software program (Nikon Corporation, Tokyo, Japan) and the levels in the control and *Pten*-cKO mice were compared. Morphological analysis was performed as described in Supplementary Methods.

BrdU labeling. The standard BrdU labeling methods that were used have been described previously[58]. Briefly, P14 and P28 mice were intraperitoneally injected with 50 μg/g of BrdU (Sigma-Aldrich Japan, Tokyo, Japan) twice at an interval of 8 h, and subjected to a histological analysis. Anti-BrdU monoclonal antibody was purchased from Roche Diagnostics Japan (Tokyo, Japan). A confocal laser scanning microscope system (A1 series, Nikon) was used to capture the microscopic images.

Western blotting. Isolated brain tissues were homogenized in ice-cold, 0.32 M sucrose buffer containing Protease Inhibitor Cocktail (Nacalai Tesque, Kyoto) and Phos STOP Phosphatase Inhibitor Cocktail (Roche). Standard techniques for western blotting were used, and detailed procedures are described in Supplementary Methods.

Drug administration. Rapamycin was injected systemically using a previously reported dosage regimen[59]. Rapamycin (LC Laboratories) was initially dissolved in 100% ethanol to a 20 mg/ml stock solution. Before injection, the stock solution was diluted in 5% Tween 80 and 5% polyethyleneglycol 400 to final concentrations of 5 mg/ml rapamycin. Rapamycin (10 mg/kg/day) or vehicle alone was intraperitoneally administered 5 days per week to mice of 6 to 9 weeks of age.

Statistical analysis. All of the statistical analyses were performed using the JMP software program (SAS Institute, Cary, NC). The collected data are presented as means ± SD unless otherwise stated. The Wilcoxon rank sum test was used as a non-parametric method. P values of < 0.05 were considered to indicate statistical significance.

References

1. Oka, E. *et al.* Prevalence of childhood epilepsy and distribution of epileptic syndromes: a population-based survey in Okayama, Japan. *Epilepsia* **47,** 626–630, doi: 10.1111/j.1528-1167.2006.00477.x (2006).
2. Russ, S. A., Larson, K. & Halfon, N. A national profile of childhood epilepsy and seizure disorder. *Pediatrics* **129,** 256–264, doi: 10.1542/peds.2010-1371 (2012).
3. Velez, A. & Eslava-Cobos, J. Epilepsy in Colombia: epidemiologic profile and classification of epileptic seizures and syndromes. *Epilepsia* **47,** 193–201, doi: 10.1111/j.1528-1167.2006.00387.x (2006).
4. Amiet, C. *et al.* Epilepsy in autism is associated with intellectual disability and gender: evidence from a meta-analysis. *Biol Psychiatry* **64,** 577–582, doi: 10.1016/j.biopsych.2008.04.030 (2008).
5. Amiet, C. *et al.* Epilepsy in simplex autism pedigrees is much lower than the rate in multiplex autism pedigrees. *Biol Psychiatry* **74,** e3–4, doi: 10.1016/j.biopsych.2013.01.037 (2013).
6. Crino, P. B. Focal brain malformations: seizures, signaling, sequencing. *Epilepsia* **50** Suppl 9, 3–8, doi: 10.1111/j.1528-1167.2009.02289.x (2009).
7. Mathern, G. W. Challenges in the surgical treatment of epilepsy patients with cortical dysplasia. *Epilepsia* **50** Suppl 9, 45–50, doi: 10.1111/j.1528-1167.2009.02294.x (2009).
8. Jamuar, S. S. & Walsh, C. A. Somatic mutations in cerebral cortical malformations. *N Engl J Med* **371,** 2038, doi: 10.1056/NEJMc1411784 (2014).
9. Jeste, S. S. & Geschwind, D. H. Disentangling the heterogeneity of autism spectrum disorder through genetic findings. *Nat Rev Neurol* **10,** 74–81, doi: 10.1038/nrneurol.2013.278 (2014).
10. Kelleher, R. J., 3rd & Bear, M. F. The autistic neuron: troubled translation? *Cell* **135,** 401–406, doi: 10.1016/j.cell.2008.10.017 (2008).
11. Lee, J. H. *et al.* De novo somatic mutations in components of the PI3K-AKT3-mTOR pathway cause hemimegalencephaly. *Nat Genet* **44,** 941–945, doi: 10.1038/ng.2329 (2012).
12. Lim, J. S. *et al.* Brain somatic mutations in MTOR cause focal cortical dysplasia type II leading to intractable epilepsy. *Nat Med*, doi: 10.1038/nm.3824 (2015).
13. Nakashima, M. *et al.* Somatic Mutations in the MTOR gene cause focal cortical dysplasia type IIb. *Ann Neurol* **78,** 375–386, doi: 10.1002/ana.24444 (2015).
14. Kyrylenko, S., Roschier, M., Korhonen, P. & Salminen, A. Regulation of PTEN expression in neuronal apoptosis. *Brain Res Mol Brain Res* **73,** 198–202 (1999).
15. Lachyankar, M. B. *et al.* A role for nuclear PTEN in neuronal differentiation. *J Neurosci* **20,** 1404–1413 (2000).
16. Backman, S. A. *et al.* Deletion of Pten in mouse brain causes seizures, ataxia and defects in soma size resembling Lhermitte-Duclos disease. *Nat Genet* **29,** 396–403, doi: 10.1038/ng782 (2001).
17. Kwon, C. H. *et al.* Pten regulates neuronal arborization and social interaction in mice. *Neuron* **50,** 377–388, doi: 10.1016/j.neuron.2006.03.023 (2006).
18. Niikura, K., Zhou, Y., Ho, A. & Kreek, M. J. Proopiomelanocortin (POMC) expression and conditioned place aversion during protracted withdrawal from chronic intermittent escalating-dose heroin in POMC-EGFP promoter transgenic mice. *Neuroscience* **236,** 220–232, doi: 10.1016/j.neuroscience.2012.12.071 (2013).
19. Padilla, S. L., Reef, D. & Zeltser, L. M. Defining POMC neurons using transgenic reagents: impact of transient Pomc expression in diverse immature neuronal populations. *Endocrinology* **153,** 1219–1231, doi: 10.1210/en.2011-1665 (2012).
20. Overstreet, L. S. *et al.* A transgenic marker for newly born granule cells in dentate gyrus. *J Neurosci* **24,** 3251–3259, doi: 10.1523/jneurosci.5173-03.2004 (2004).
21. Baram, T. Z. Pathophysiology of massive infantile spasms: perspective on the putative role of the brain adrenal axis. *Ann Neurol* **33,** 231–236, doi: 10.1002/ana.410330302 (1993).
22. Brunson, K. L., Avishai-Eliner, S. & Baram, T. Z. ACTH treatment of infantile spasms: mechanisms of its effects in modulation of neuronal excitability. *Int Rev Neurobiol* **49,** 185–197 (2002).
23. Groszer, M. *et al.* Negative regulation of neural stem/progenitor cell proliferation by the Pten tumor suppressor gene *in vivo*. *Science* **294,** 2186–2189, doi: 10.1126/science.1065518 (2001).
24. Pun, R. Y. *et al.* Excessive activation of mTOR in postnatally generated granule cells is sufficient to cause epilepsy. *Neuron* **75,** 1022–1034, doi: 10.1016/j.neuron.2012.08.002 (2012).
25. Buckmaster, P. S. & Lew, F. H. Rapamycin suppresses mossy fiber sprouting but not seizure frequency in a mouse model of temporal lobe epilepsy. *J Neurosci* **31,** 2337–2347, doi: 10.1523/JNEUROSCI.4852-10.2011 (2011).
26. Kwak, S. P., Morano, M. I., Young, E. A., Watson, S. J. & Akil, H. Diurnal CRH mRNA rhythm in the hypothalamus: decreased expression in the evening is not dependent on endogenous glucocorticoids. *Neuroendocrinology* **57,** 96–105 (1993).
27. Williams, M. R., DeSpenza, T., Jr., Li, M., Gulledge, A. T. & Luikart, B. W. Hyperactivity of newborn Pten knock-out neurons results from increased excitatory synaptic drive. *J Neurosci* **35,** 943–959, doi: 10.1523/JNEUROSCI.3144-14.2015 (2015).
28. Ljungberg, M. C., Sunnen, C. N., Lugo, J. N., Anderson, A. E. & D'Arcangelo, G. Rapamycin suppresses seizures and neuronal hypertrophy in a mouse model of cortical dysplasia. *Dis Model Mech* **2,** 389–398, doi: 10.1242/dmm.002386 (2009).
29. Sunnen, C. N. *et al.* Inhibition of the mammalian target of rapamycin blocks epilepsy progression in NS-Pten conditional knockout mice. *Epilepsia* **52,** 2065–2075, doi: 10.1111/j.1528-1167.2011.03280.x (2011).
30. Blumcke, I. *et al.* The clinicopathologic spectrum of focal cortical dysplasias: a consensus classification proposed by an ad hoc Task Force of the ILAE Diagnostic Methods Commission. *Epilepsia* **52,** 158–174, doi: 10.1111/j.1528-1167.2010.02777.x (2011).
31. Zucca, I. *et al.* Type II FCD: *ex vivo* 7 Tesla MRI abnormalities and histopathological comparisons. *Ann Neurol*, doi: 10.1002/ana.24541 (2015).
32. Sisodiya, S. M., Fauser, S., Cross, J. H. & Thom, M. Focal cortical dysplasia type II: biological features and clinical perspectives. *Lancet Neurol* **8,** 830–843, doi: 10.1016/S1474-4422(09)70201-7 (2009).
33. Ljungberg, M. C. *et al.* Activation of mammalian target of rapamycin in cytomegalic neurons of human cortical dysplasia. *Ann Neurol* **60,** 420–429, doi: 10.1002/ana.20949 (2006).
34. Cepeda, C., Andre, V. M., Vinters, H. V., Levine, M. S. & Mathern, G. W. Are cytomegalic neurons and balloon cells generators of epileptic activity in pediatric cortical dysplasia? *Epilepsia* **46** Suppl 5, 82–88, doi: 10.1111/j.1528-1167.2005.01013.x (2005).
35. Kjeldsen, M. J., Kyvik, K. O., Christensen, K. & Friis, M. L. Genetic and environmental factors in epilepsy: a population-based study of 11900 Danish twin pairs. *Epilepsy Res* **44,** 167–178 (2001).
36. Fahrner, A. *et al.* Granule cell dispersion is not accompanied by enhanced neurogenesis in temporal lobe epilepsy patients. *Exp Neurol* **203,** 320–332, doi: 10.1016/j.expneurol.2006.08.023 (2007).
37. D'Alessio, L. *et al.* Doublecortin (DCX) immunoreactivity in hippocampus of chronic refractory temporal lobe epilepsy patients with hippocampal sclerosis. *Seizure* **19,** 567–572, doi: 10.1016/j.seizure.2010.09.004 (2010).
38. Sosunov, A. A. *et al.* The mTOR pathway is activated in glial cells in mesial temporal sclerosis. *Epilepsia* **53** Suppl 1, 78–86, doi: 10.1111/j.1528-1167.2012.03478.x (2012).
39. Hamano, S. *et al.* Interictal cerebral blood flow abnormality in cryptogenic West syndrome. *Epilepsia* **51,** 1259–1265, doi: 10.1111/j.1528-1167.2009.02495.x (2010).
40. Wang, W., Murphy, B., Dow, K. E., David Andrew, R. & Fraser, D. D. Systemic adrenocorticotropic hormone administration down-regulates the expression of corticotropin-releasing hormone (CRH) and CRH-binding protein in infant rat hippocampus. *Pediatr Res* **55,** 604–610, doi: 10.1203/01.PDR.0000112105.33521.DC (2004).

41. Galanopoulou, A. S. Basic mechanisms of catastrophic epilepsy–overview from animal models. *Brain Dev* **35,** 748–756, doi: 10.1016/j.braindev.2012.12.005 (2013).
42. Cowley, M. A. *et al.* Leptin activates anorexigenic POMC neurons through a neural network in the arcuate nucleus. *Nature* **411,** 480–484, doi: 10.1038/35078085 (2001).
43. Caruso, V., Lagerstrom, M. C., Olszewski, P. K., Fredriksson, R. & Schioth, H. B. Synaptic changes induced by melanocortin signalling. *Nat Rev Neurosci* **15,** 98–110 (2014).
44. Caruso, C. *et al.* Melanocortin 4 receptor activation induces brain-derived neurotrophic factor expression in rat astrocytes through cyclic AMP-protein kinase A pathway. *Mol Cell Endocrinol* **348,** 47–54, doi: 10.1016/j.mce.2011.07.036 (2012).
45. Ito, M. Extremely low-dose ACTH therapy for West syndrome in Japan. *Brain Dev* **23,** 635–641 (2001).
46. D'Gama, A. M. *et al.* Mammalian target of rapamycin pathway mutations cause hemimegalencephaly and focal cortical dysplasia. *Ann Neurol* **77,** 720–725, doi: 10.1002/ana.24357 (2015).
47. Krueger, D. A. *et al.* Everolimus treatment of refractory epilepsy in tuberous sclerosis complex. *Ann Neurol* **74,** 679–687, doi: 10.1002/ana.23960 (2013).
48. Abdijadid, S., Mathern, G. W., Levine, M. S. & Cepeda, C. Basic mechanisms of epileptogenesis in pediatric cortical dysplasia. *CNS Neurosci Ther* **21,** 92–103, doi: 10.1111/cns.12345 (2015).
49. Lasarge, C. L. & Danzer, S. C. Mechanisms regulating neuronal excitability and seizure development following mTOR pathway hyperactivation. *Front Mol Neurosci* **7,** 18, doi: 10.3389/fnmol.2014.00018 (2014).
50. Supekar, K. *et al.* Brain hyperconnectivity in children with autism and its links to social deficits. *Cell Rep* **5,** 738–747, doi: 10.1016/j.celrep.2013.10.001 (2013).
51. Tye, C. & Bolton, P. Neural connectivity abnormalities in autism: insights from the Tuberous Sclerosis model. *BMC Med* **11,** 55, doi: 10.1186/1741-7015-11-55 (2013).
52. Sakai, Y. *et al.* Protein interactome reveals converging molecular pathways among autism disorders. *Sci Transl Med* **3,** 86ra49, doi: 10.1126/scitranslmed.3002166 (2011).
53. Bolton, P. F., Park, R. J., Higgins, J. N., Griffiths, P. D. & Pickles, A. Neuro-epileptic determinants of autism spectrum disorders in tuberous sclerosis complex. *Brain* **125,** 1247–1255 (2002).
54. Suzuki, A. *et al.* T cell-specific loss of Pten leads to defects in central and peripheral tolerance. *Immunity* **14,** 523–534 (2001).
55. McHugh, T. J. *et al.* Dentate gyrus NMDA receptors mediate rapid pattern separation in the hippocampal network. *Science* **317,** 94–99, doi: 10.1126/science.1140263 (2007).
56. Takase, K. *et al.* Prenatal freeze lesioning produces epileptogenic focal cortical dysplasia. *Epilepsia* **49,** 997–1010, doi: 10.1111/j.1528-1167.2008.01558.x (2008).
57. Sakai, Y. *et al.* Neuroendocrine phenotypes in a boy with 5q14 deletion syndrome implicate the regulatory roles of myocyte-specific enhancer factor 2C in the postnatal hypothalamus. *Eur J Med Genet* **56,** 475–483, doi: 10.1016/j.ejmg.2013.06.009 (2013).
58. Yutsudo, N. *et al.* FosB-null mice display impaired adult hippocampal neurogenesis and spontaneous epilepsy with depressive behavior. *Neuropsychopharmacology* **38,** 895–906, doi: 10.1038/npp.2012.260 (2013).
59. Zeng, L. H., Xu, L., Gutmann, D. H. & Wong, M. Rapamycin prevents epilepsy in a mouse model of tuberous sclerosis complex. *Ann Neurol* **63,** 444–453, doi: 10.1002/ana.21331 (2008).

Acknowledgements

We thank Christian P. Schaaf at the Neurological Research Institute, Texas Children's Hospital for the critical reading and helpful comments on this manuscript; Etsuro Ono and technical staffs for maintaining the mice at the Animal Core Facility of Kyushu University; Satoshi Tamura and Masako Ino (Nikon) for performing the morphological analyses; Junji Kishimoto (Kyushu University) for the statistical analysis; Setsuko Kitamura, Tamami Tanaka and Ayumi Tahara for their technical support (Kyushu University); Ryutaro Kira (Fukuoka Children's Hospital), and the laboratory members for their helpful discussions. This work was supported by JSPS KAKENHI Grant Numbers 24650199 (YS), 22221004 (YN) and 26461547 (YI); Japan Life Science Foundation (YS); Takeda Science Foundation (YS); The Mother and Child Health Foundation (YS); and the Japan Epilepsy Research Foundation (YS).

Author Contributions

Y.M. conceived and Y.S. supervised the experiments. Y.M. and Y.S. wrote the manuscript. M.S. and H.S. supported the EEG recordings. S.A., M.S., Y.I. and H.T. assisted experiments and data analyses. M.N., Y.N. and A.S. provided supports for mouse works and microscopic studies. Y.S., H.T. and T.H. directed this study.

Additional Information

Supplementary information accompanies this paper at http://www.nature.com/srep

Competing financial interests: The authors declare no competing financial interests.

How to cite this article: Matsushita, Y. *et al.* Hyperactive mTOR signals in the proopiomelanocortin-expressing hippocampal neurons cause age-dependent epilepsy and premature death in mice. *Sci. Rep.* **6**, 22991; doi: 10.1038/srep22991 (2016).

SCIENTIFIC REPORTS

OPEN

Corrigendum: Hyperactive mTOR signals in the proopiomelanocortin-expressing hippocampal neurons cause age-dependent epilepsy and premature death in mice

Yuki Matsushita, Yasunari Sakai, Mitsunori Shimmura, Hiroshi Shigeto, Miki Nishio, Satoshi Akamine, Masafumi Sanefuji, Yoshito Ishizaki, Hiroyuki Torisu, Yusaku Nakabeppu, Akira Suzuki, Hidetoshi Takada & Toshiro Hara

Scientific Reports **6**:22991; doi: 10.1038/srep22991; published online 10 March 2016; updated 10 June 2016

In Figure 2b and 2c, the electroencephalogram scale '500 μV' is incorrectly given as '500 mV'. The correct Figure 2 appears below as Figure 1.

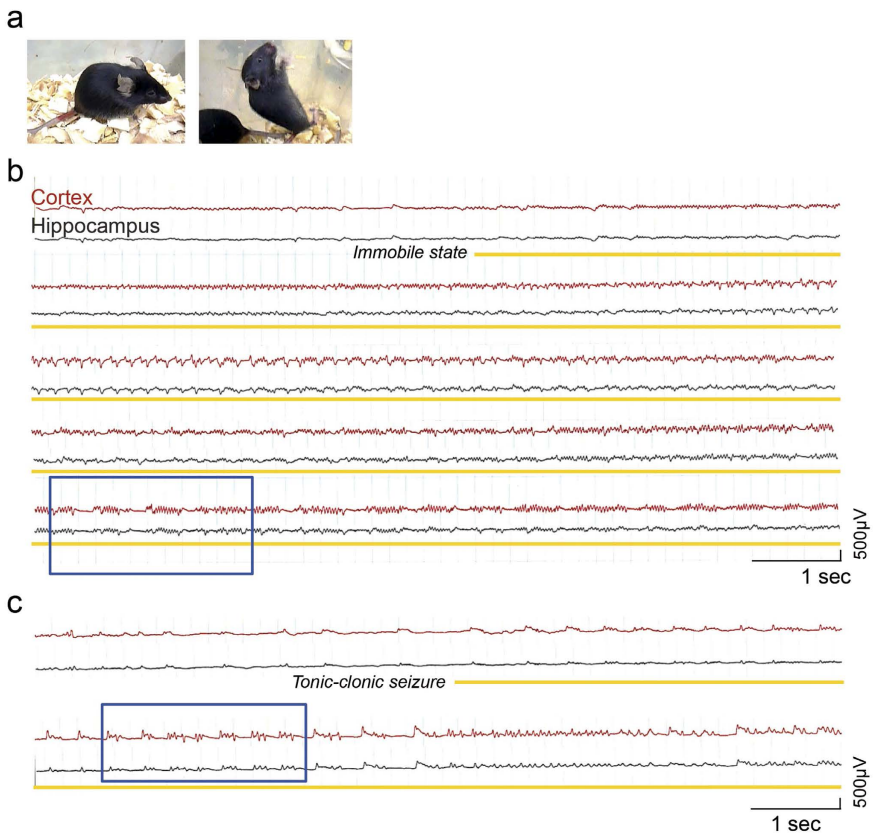

Figure 1.

Supplementary Information for:

Hyperactive mTOR signals in the proopiomelanocortin-expressing hippocampal neurons cause age-dependent epilepsy and premature death in mice

Yuki Matsushita, Yasunari Sakai, Mitsunori Shimmura, Hiroshi Shigeto, Miki Nishio, Satoshi Akamine, Masafumi Sanefuji, Yoshito Ishizaki, Hiroyuki Torisu, Yusaku Nakabeppu, Akira Suzuki, Hidetoshi Takada, Toshiro Hara

This file contains:
Supplementary Figures S1-S7 and their legends
Supplementary Tables S1, S2
Supplementary Methods
Captions for Supplementary Videos S1, S2

a

Generation	Genotype
F0	*Pomc-Cre*$^{Tg/+}$ *Pten-flox/+*
F1	*Pomc-Cre*$^{+/+}$;*Pten*+/+ *Pomc-Cre*$^{Tg/+}$;*Pten*+/+ *Pomc-Cre*$^{+/+}$;*Pten-flox/+* *Pomc-Cre*$^{Tg/+}$;*Pten-flox/+*
F2	*Pomc-Cre*$^{+/+}$;*Pten*+/+ *Pomc-Cre*$^{Tg/+}$;*Pten*+/+ *Pomc-Cre*$^{+/+}$;*Pten-flox/+* *Pomc-Cre*$^{Tg/+}$;*Pten-flox/flox* (*Pten*-cKO) *Pomc-Cre*$^{+/+}$;*Pten-flox/flox* (Control) *Pomc-Cre*$^{Tg/+}$;*Pten-flox/+*

b

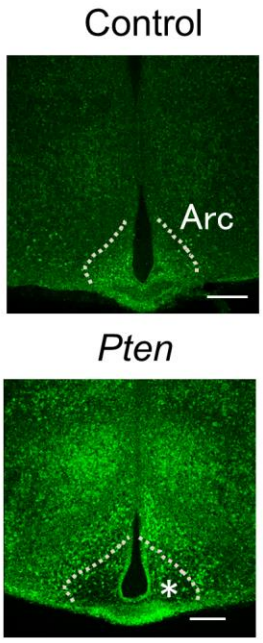

c

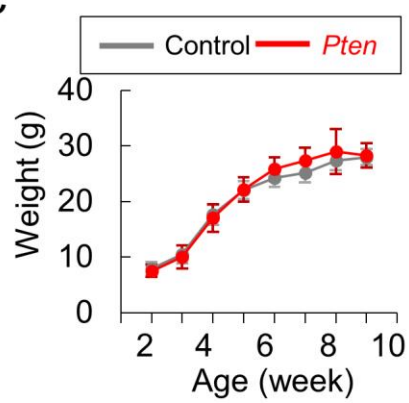

d

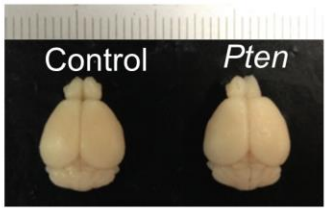

e

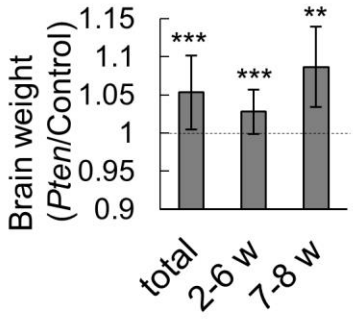

f

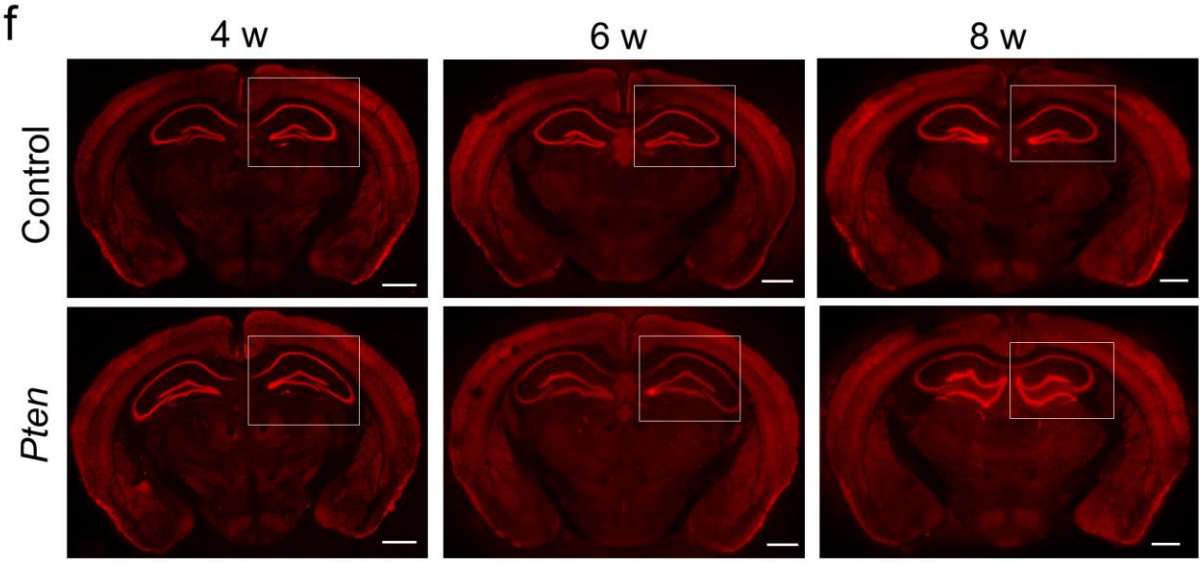

Supplementary Figure S1. Overgrowth of the *Pten*-cKO brain

(a) The mating scheme. By mating the *Pomc-Cre*$^{Tg/+}$ and *Pten-flox/+* lines (F0), heterozygous (*Pomc-Cre*$^{Tg/+}$;*Pten+/+ and Pomc-Cre*$^{+/+}$;*Pten-flox/+*) and double-heterozygous mice (*Pomc-Cre*$^{Tg/+}$;*Pten-flox/+*) were obtained (F1). The next round of mating yielded *Pten*-cKO (*Pomc-Cre*$^{Tg/+}$;*Pten-flox/flox*) and control mice (*Pomc-Cre*$^{+/+}$;*Pten-flox/flox*) (F2). The mated pairs (blue) and the mice used in this study (red, control and *Pten*-cKO mice) are highlighted with colored fonts.

(b) Deficient Pten expression in the hypothalamic arcuate nuclei of *Pten*-cKO mice. Coronary sections from 4-week-old control and *Pten*-cKO mice (*Pten*), were dissected. Asterisks indicate the ablated Pten signals (green) in the arcuate nuclei (Arc) of a *Pten*-cKO mouse. Dashed lines indicate the boundary of the Arc. Scale bar, 200 μm.

(c) The growth curve for control (n = 31) and *Pten*-cKO male mice (n = 28).

(d) Whole brains dissected from control and *Pten*-cKO mice at 8 weeks of age.

(e) The overgrowth of the *Pten*-cKO brains. The relative ratios of the brain weight for the *Pten*-cKO mice (n = 18) to that of control mice (n= 15) are shown in the bar plot. Brains from *Pten*-cKO mice weighed significantly more than the brains of littermate controls at two different time points (Wilcoxon rank sum test; P values of <0.0001 in total, 0.0002 at 2-6 weeks, and 0.0028 at 7-8 weeks of age). **P <0.01, ***P <0.001. The plotted values show the means ± SD.

(f) An overview of the NeuN signals (red) in the whole coronary sections from the control (upper) and *Pten*-cKO (lower) mice at different ages. Note that the DG became prominently hypertrophic at 4-6 weeks of age. Scale bar, 1 mm.

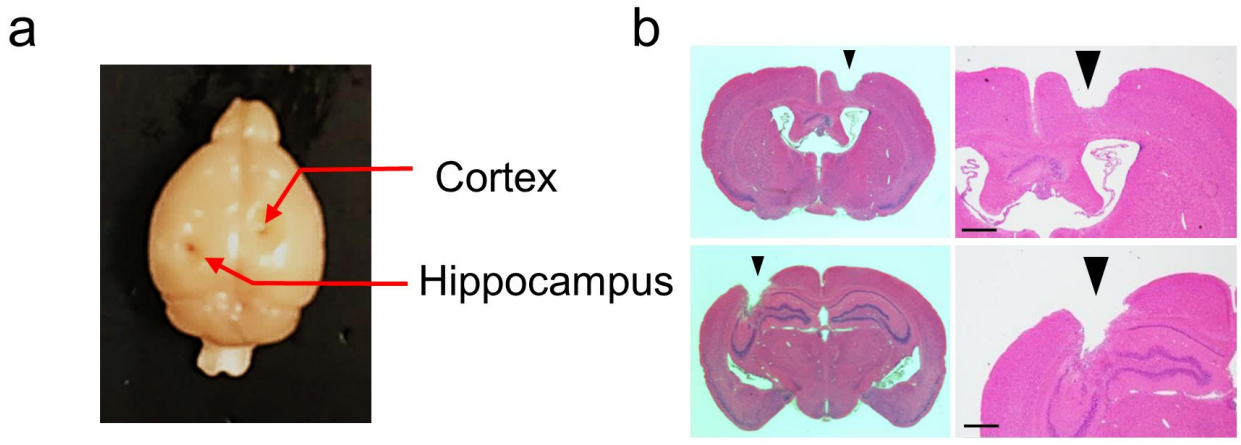

Supplementary Figure S2. The post-operational dissection of the *Pten*-cKO mouse

brain

(a) The whole-brain appearance of a *Pten*-cKO mouse after EEG recording at 10 weeks of age. Annotations indicate the positions of the cortical and hippocampal electrodes.

(b) The HE staining of a coronal section shows that the surface and deep electrode were both correctly inserted into the cerebral cortex (upper) and hippocampus (lower). The insertion points of the electrodes (arrowheads) are shown with higher magnification in the two images on the far right. Scale bar, 500 μm.

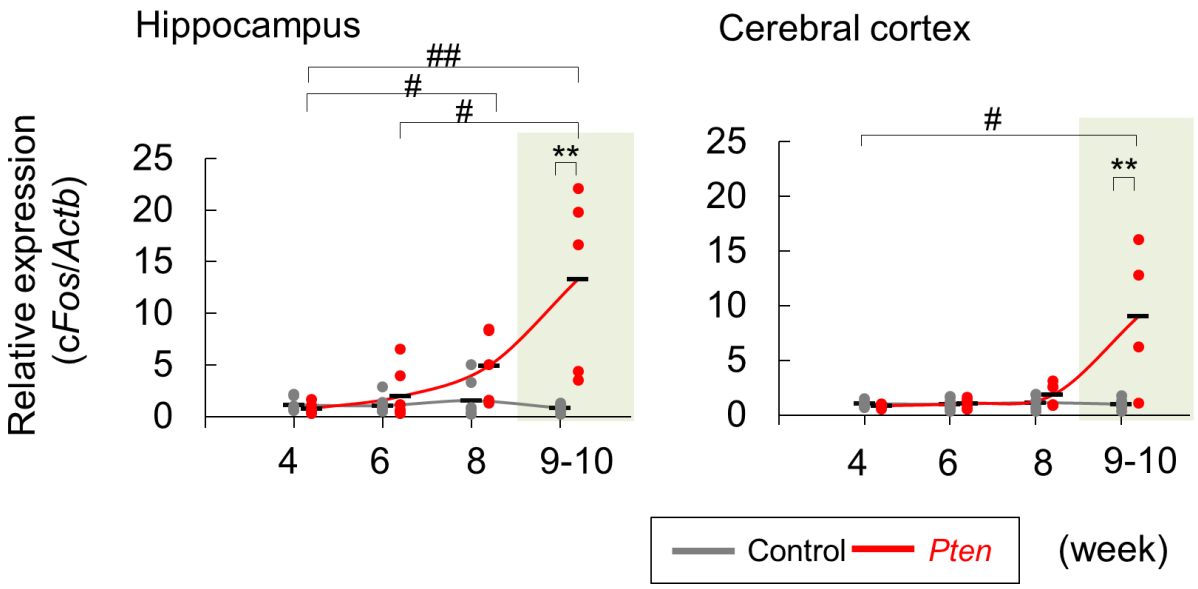

Supplementary Figure S3. The time course of *cFos* expression in the hippocampus and cerebral cortex

The increase in *cFos* mRNA expression in the hippocampus (left) of the *Pten*-cKO mice preceded that in the cerebral cortex (right). The control mice did not show such a similar increase in this period (4-10 weeks). The plots present the data from 3 or more pairs of littermates at each time point. The horizontal bars denote the average of the plots. Asterisks (*) indicate a statistically significant difference between different genotypes. Hashes (#) indicate a statistically significant difference between different time points. $P < 0.05$ (* and #), $P < 0.01$ (** and ##). *cFos* expression was normalized with the expression of *Actb*.

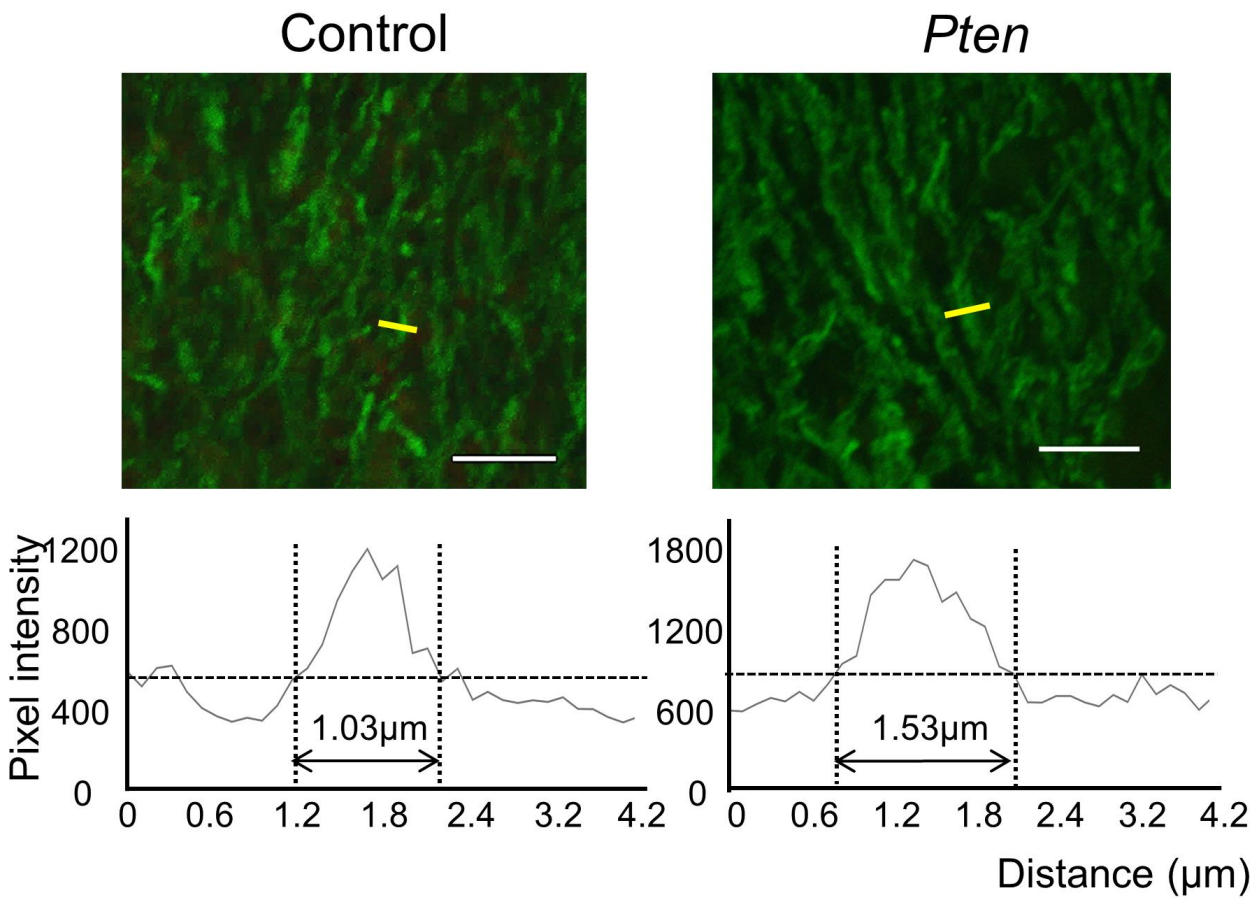

Supplementary Figure S4. The quantitative analysis of dendrite width

The upper panels show the fluorescence signal of Map2 (green) in the molecular layer of the DG. Four-week-old control and *Pten*-cKO mice were used for this assay. Optical cross-sections were set at right angles to the long axis of the dendritic shaft for the quantitative analysis of the dendritic width (yellow lines). The lower panels depict the contour plots for the quantitated Map2 signal. The width of each dendrite was measured using the standard full width at half maximum (FWHM) method, as shown in the lower panels. Scale bar (white line), 10 μm.

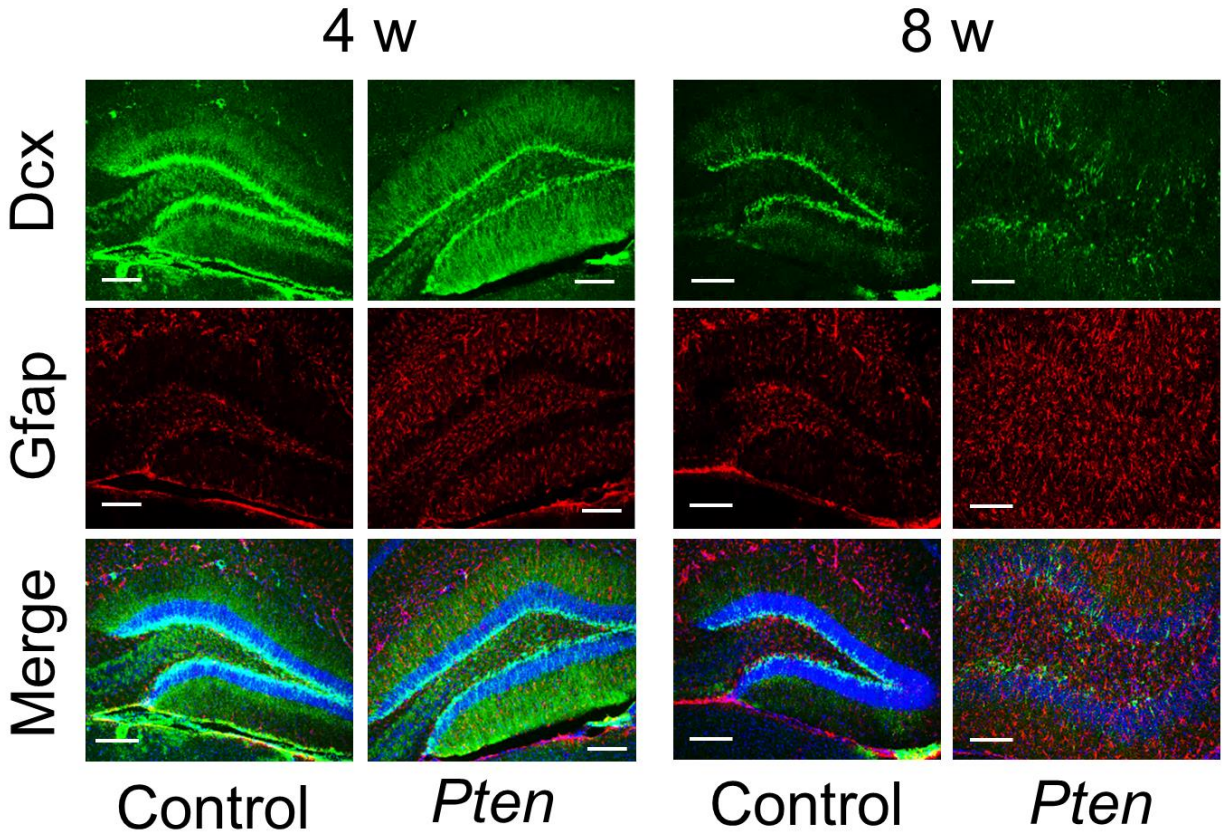

Supplementary Figure S5. Impaired neuronal differentiation in the hippocampal DG of *Pten*-cKO mice

The panels show the Dcx (green) and Gfap (red) signals in the DG of control and *Pten*-cKO mice at 4 and 8 weeks of age. Note that the Dcx signals peak at the subgranular layer in the control mice, whereas the Dcx signals are sparse in the DG of *Pten*-cKO mice at 8 weeks of age. The progressive increases in the Gfap signals during this timeframe are also presented. Scale bar, 200 μm.

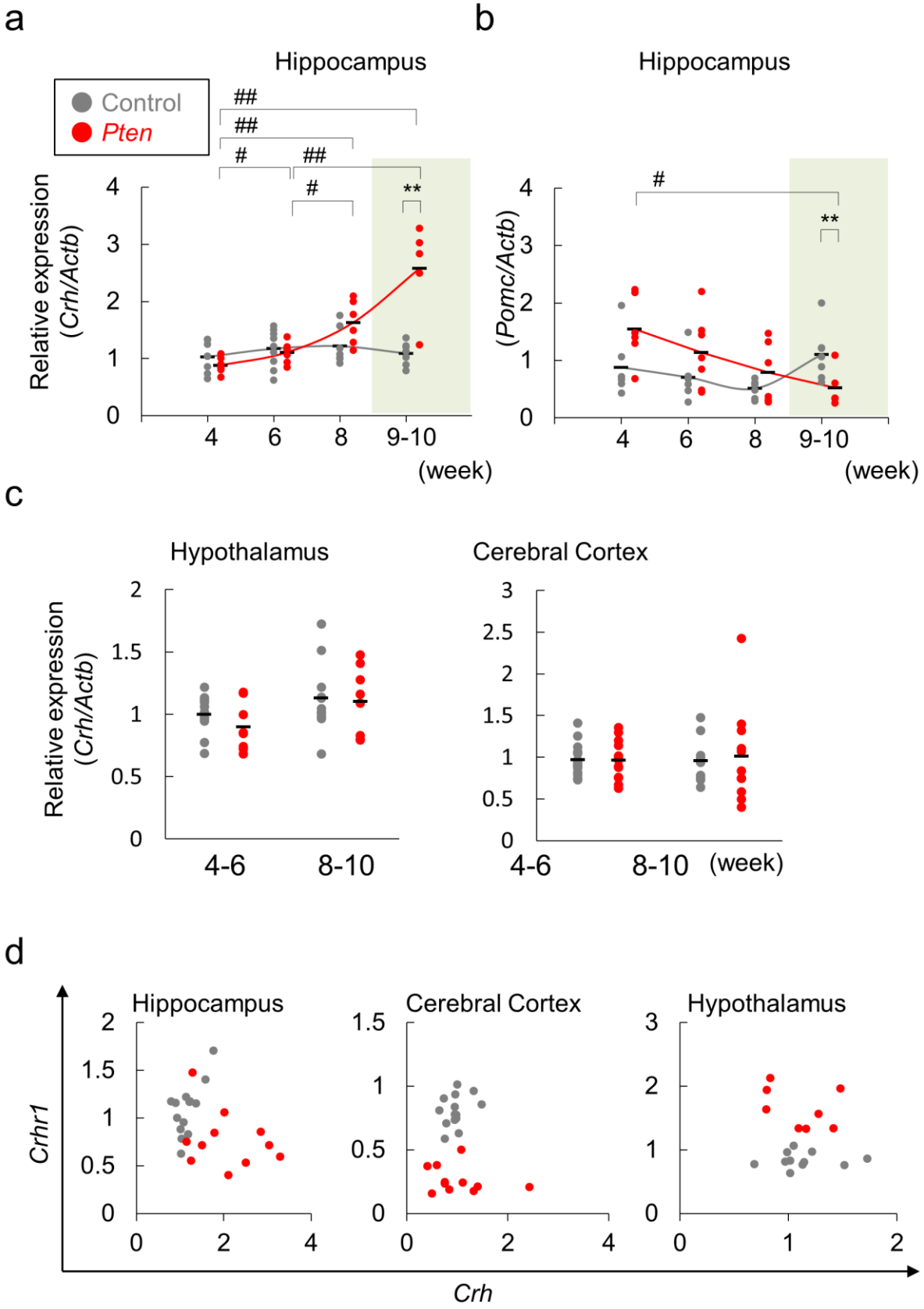
a
Hippocampus
Control
Pten
##
##
#
##
#
**
Relative expression
(Crh/Actb)
4
3
2
1
0
4
6
8
9-10
(week)
b
Hippocampus
#
**
(Pomc/Actb)
4
3
2
1
0
4
6
8
9-10
(week)
c
Hypothalamus
Relative expression
(Crh/Actb)
2
1.5
1
0.5
0
4-6
8-10
Cerebral Cortex
3
2.5
2
1.5
1
0.5
0
4-6
8-10
(week)
d
Hippocampus
Cerebral Cortex
Hypothalamus
Crhr1
Crh
2
1.5
1
0.5
0
0
2
4
1.5
1
0.5
0
0
2
4
3
2
1
0
0
1
2

Supplementary Figure S6. Aberrant *Crh, Pomc* and *Crhr1* expression in *Pten*-cKO mice

(a, b) The time course of *Crh* (a) and *Pomc* (b) mRNA expression in the hippocampus. Asterisks (*) indicate a statistically significant difference between different genotypes. Hashes (#) indicate a statistically significant difference between different ages. # P < 0.05; ** and ## P < 0.01.

(c) Unaltered *Crh* expressions in the hypothalamus and cerebral cortex of control and *Pten*-cKO mice before and after the onset of seizures.

(d) The co-expression profiles for *Crh* and *Crhr1* mRNAs in the hippocampus, cerebral cortex and hypothalamus of control and *Pten*-cKO mice.

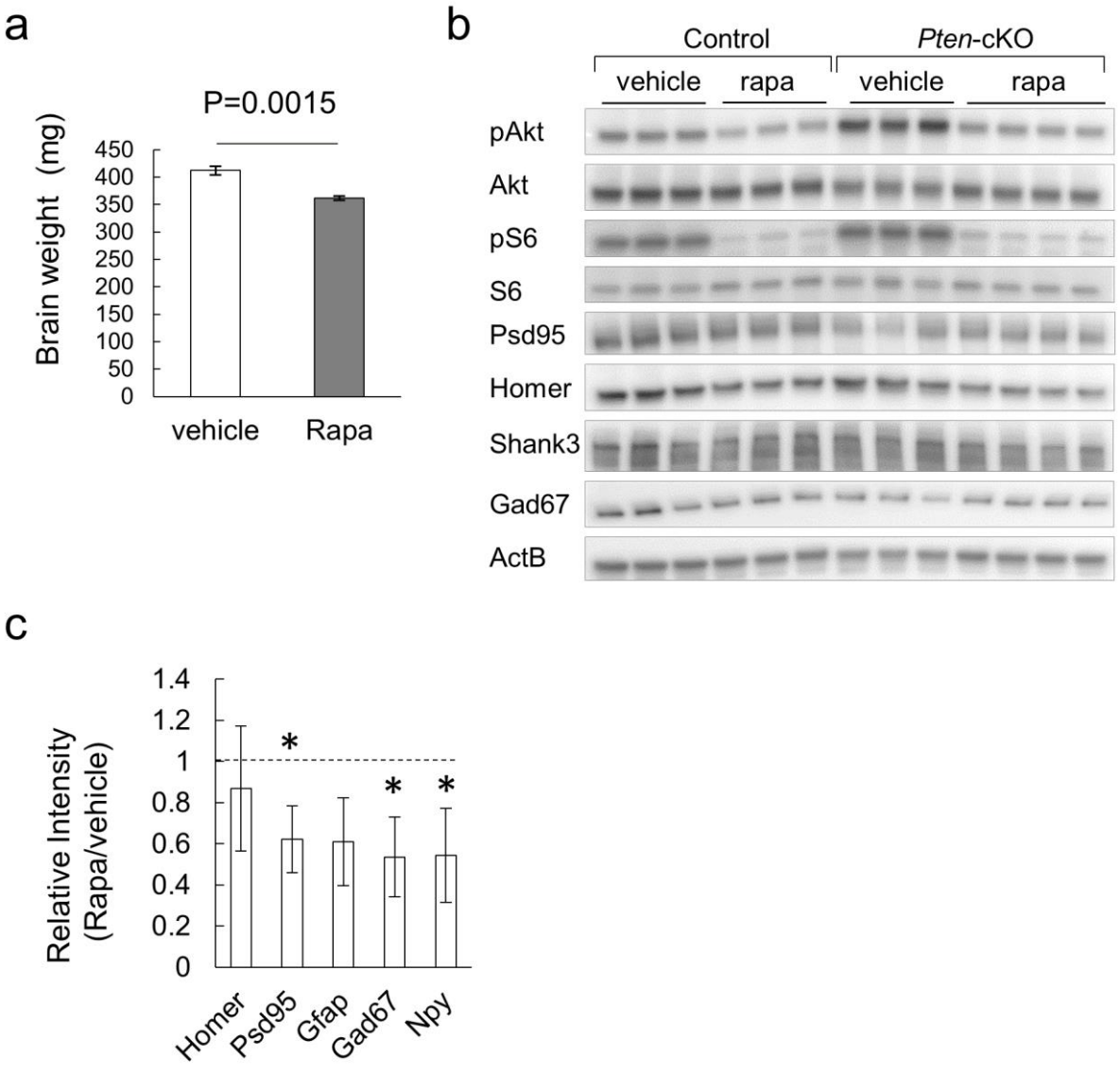

Supplementary Figure S7. Rapamycin reverses the phenotypes of *Pten*-cKO mice

(a) The total weight of the brain from vehicle or rapamycin-treated *Pten*-cKO mice. Whole brains were dissected at 9 weeks of age after vehicle (n = 3) or rapamycin (n = 3) treatment.

(b) Western blotting for the hippocampal extracts from vehicle- or rapamycin-treated *Pten*-cKO mice. The protein signals on these blots were used for a quantitative analysis. The measured signal intensity for each protein was normalized with that of Actb. The mean values obtained from vehicle-treated control mice were used as reference values (value: 1 for each protein). The quantitated data were plotted (Fig. 5b).

(c) The relative fluorescence signals of the marker proteins. Three pairs of *Pten*-cKO mice with or without rapamycin treatment were subjected to an immunofluorescence analysis. The fluorescence signals of each protein in the regions of interest (squared regions in Fig. 5d) were measured and plotted as the mean ± SD. * $P < 0.05$.

Supplementary Table S1. The oligonucleotide primers used for the quantitative PCR analyses

Gene	Forward (5' to 3')	Reverse (5' to 3')
Pten	CGGAACTTGCAATCCTCAGT	AATGGCTGAGGGAACTCAAA
Gfap	AAGCCAAGCACGAAGCTAAC	CATTTGCCGCTCTAGGGACTC
Psd95	GCCTAAAGGACTTGGCTTCA	GGATCTTGTCTCCGATCTGC
Shank3	TGCAGCAGCTGAATAAAGACA	TGAGATGGTGCTCAGCTCAC
Shank1	CAAAGACTGGGTTGAAGAAG	GGTGTCTCTCCTGAATCTGA
Homer1	CAGTTTAGATGGCTCAAAGG	AAGATGATGCTCAGAGGAGA
Grm5	AGCAAGTGATCAGAAAGACTCG	GTCACAGACTGCAGCAGAGC
Cntnap2	CTTGGCACCTAGATCACTTG	CCTCCAATGATAGCTGAGTT
Nlgn3	CATCCTGTGTCAGTCTCCTT	TCACTGGTTGGTAGTTCACA
Pvalb	CGCTGAGGACATCAAGAAGG	CCGGGTTCTTTTTCTTCAGG
Gad67	CAAACTCAGCGGCATAGAAA	GAAGAGGTAGCCTGCACACA
Gphn	AGGATCTCAGGAATGCTTTC	CTTCAAGTTCATCATGCACC
Crh	GCAGTTAGCTCAGCAAGCTCAC	CAAATGATATCGGAGCTGCG
Crhr1	AAGTGGATGTTCGTCTGCAT	CCAAACCAGCACTTTTCATT
Mc4r	TCTCTATGTCCACATGTTCCTG	GGGGCCCAGCAGACAACAAAG
cFos	GAGGAAGAGAAACGGAGAAT	GTCTCCGCTTGGAGTGTAT
Actb	TTGGGTATGGAATCCTGTGG	CTTCTGCATCCTGTCAGCAA

Supplementary Table S2. The primary antibodies used in the present study

Antigen	Host	Supplier	Cat.#	IF	WB
Pten	Rb	Cell Signaling Technology	#9188	1/100	1/1000
Akt	Rb	Cell Signaling Technology	#4691	1/1000	1/1000
pAkt(Ser473)	Rb	Cell Signaling Technology	#4060	1/100	1/2000
S6	Rb	Cell Signaling Technology	#2217	1/1000	1/1000
pS6(Ser240/244)	Rb	Cell Signaling Technology	#5364	1/1000	1/1000
NeuN	Ms	Merck Millipore	MAB377	1/3000	-
cFos	Rb	Santa Cruz Biotechnology	sc-52	1/1000	-
Npy	Rb	Santa Cruz Biotechnology	sc-133080	1/100	-
Homer	Rb	Santa Cruz Biotechnology	sc-15321	1/500	1/200
Psd95	Ms	Abcam	ab2723	1/1000	1/500
Gfap	Ms	Sigma	G3893	1/5000	1/5000
Shank3	Rb	Santa Cruz Biotechnology	sc-30193	-	1/200
Gad67	Ms	Millipore	MAB5406	1/15000	1/5000
Map2	Rb	Abcam	ab32454	1/100	-
BrdU	Ms	Roche Diagnostic Japan	BMC9318	1/1000	-
Dcx	Goat	Santa Cruz Biotechnology	sc-8066	1/100	-
Znt3	Rb	Synaptic Systems	197 002	1/500	-

IF, immunofluorescence; WB, western blot; -, not used

Supplementary Methods

Genotyping

Genotyping PCR using the genomic DNA was performed as described (Chao et al., 2010). Following primers to amplify transgene (Cre) and internal positive control gene (PC) were used: (Cre-for) 5'-CCATCTGCCACCAGCCAG-3' and (Cre-rev) 5'-TCGCCATCTTCCAGCAGG-3'; (PC-for) 5'-ACTGGGATCTTCGAACTCTTTGGAC-3' and (PC-rev) 5'-GATGTTGGGGCACTGCTCATTCACC-3'. *Pten-flox* alleles were detected with the following primers (Flox-for) 5'-GTGAAAGTGCCCCAACATAAGG-3' and (Flox-rev) 5'-CTCCCACCAATGAACAAACAGTC-3'.

Surgical operation for the electrode placement

A mouse was fixed on a stereotactic frame and the head skin was cut to expose the cranium. A stainless steel screw electrode was placed at subdural point of the right parietal lobe (1 mm posterior to the Bregma and 1 mm lateral from the midline). A depth-recording electrode, which was made of twisted nichrome wire (diameter 0.02 mm), was inserted into the CA3 regions of the left hippocampus (3 mm posterior from the Bregma, 3 mm lateral to the midline, and 2 mm deep from the cortical surface). A reference screw electrode was placed on the parietal bone. All electrodes were connected to a 2-channel amplifier (MEG-6168, Nihon Kohden, Tokyo).

Western blotting

Twenty-five µg of total protein was applied for SDS-PAGE using 4-15% Mini-PROTEAN TGX Gels (BioRad). Separated proteins were transferred to PVDF membranes (Trans-Blot Turbo Transfer Pack, BioRad). The blotted membranes were blocked with 5% milk and incubated overnight at 4˚C with primary antibodies (Supplementary Table S2). Secondary antibodies conjugated to horseradish peroxidase (211-032-171 or 115-035-174, Jackson ImmunoResearch, West Grove, PA) were used to detect chemiluminescence (Clarity ECL substrate, BioRad, and ImmunoStar LD, Wako). All measurements were performed using the FluorChem FC2 System software program (ProteinSimple, San Jose, CA, USA). Beta-Actin (Actb) was used as an internal control.

Morphological analysis

Neurons in the granule cell layer of the dentate gyrus were analyzed with a confocal laser microscopic system. For each targeted region of interest, a total of 20 XY-plane images were captured at 0.13 µm per step for the Z-axis (2.6 µm of thickness) with a 100x objective lens (Nikon, CFI Plan Apo VC 100xH). Stacked images were projected onto one XY-plane,

and the resulting image was used for the morphological analyses. The dendrite width was measured with the full width at half maximum (FWHM) method, as previously described [1]. Briefly, 15-20 regions of interest (ROIs) were set on an XY plane, and the Map2 signal intensity was converted to a contour-tracing plot on an optical cross-section of a target dendrite. The cross-section line for a dendritic shaft was drawn with a right angle to the longitudinal axis of the target dendrite (Supplementary Fig. S4). The size of the soma was determined by measuring the total surface area of nuclei with NeuN-positive signals in the granule cell layer using the NIS-elements AR software program (Nikon corporation, Tokyo, Japan). Distances between two nuclei were also measured for each ROI and the results were consistent with an independent method based on the size of the NeuN-positive nuclei. Data from 12 confocal images were collected from at least 3 pairs of *Pten*-cKO and control littermates.

Supplementary Reference

1. Nagerl UV, Willig KI, Hein B, Hell SW, Bonhoeffer T. Live-cell imaging of dendritic spines by STED microscopy. *Proc Natl Acad Sci U S A* **105,** 18982-18987 (2008).

Caption for Supplementary Videos.

The two types of seizure pattern. Two movies are provided to show the unique seizure patterns of a female *Pten*-cKO mouse at nine weeks of age. Digital video images were processed using the Super Media Converter software program (Wondershare Software, Tokyo). The EEG recordings for Supplementary Video S1 and S2 are presented in Fig. 2b and Fig. 2c, respectively.

Supplementary Video S1. The unresponsive, immobile seizure pattern: This movie (0'40") starts with the normal behavior of a *Pten*-cKO mouse (0'00"-0'04"). The mouse stops moving with intermittent sniffing.

Supplementary Video S2. A generalized tonic-clonic seizure: This movie (0'38") shows a generalized tonic-clonic seizure (0'13"-0'32") which includes head nodding, tonic posture, ramping and falling backwards with forelimb clonus. The seizure ends with the mouse standing up again, breathing heavily and intermittent forelimb clonus.